Characterization of *Spiroplasma citri* MreB1

A Thesis

submitted to

Indian Institute of Science Education and Research Pune in partial fulfilment of the requirements for the BS-MS Dual Degree Programme

by

Akhilesh Uthaman

Indian Institute of Science Education and Research Pune

Dr. Homi Bhabha Road,

Pashan, Pune 411008, INDIA.

Date: April, 2023

Under the guidance of

Supervisor: **Dr. Gayathri Pananghat**

Associate Professor

From May 2022 to Mar 2023

INDIAN INSTITUTE OF SCIENCE EDUCATION AND RESEARCH PUNE

Certificate

This is to certify that this dissertation entitled "**Characterization of *Spiroplasma citri* MreB1"** towards the partial fulfilment of the BS-MS dual degree programme at the Indian Institute of Science Education and Research, Pune represents study/work carried out by Akhilesh Uthaman at Indian Institute of Science Education and Research under the supervision of Dr Gayathri Pananghat, Associate Professor, Department of Biology, during the academic year 2022-23.

Dr. Gayathri Pananghat

Committee:

Dr. Gayathri Pananghat

Dr. Sunish Radhakrishnan

Declaration

I hereby declare that the matter embodied in the report entitled "**Characterization of *Spiroplasma citri* MreB1"** are the results of the work carried out by me at the Department of Biology, Indian Institute of Science Education and Research, Pune, under the supervision of Dr Gayathri Pananghat and the same has not been submitted elsewhere for any other degree

Akhilesh Uthaman

Date: 10/04/2023

Table of Contents

Title **Page**

List of Tables

Page

List of Figures

Page

Abstract

For a living cell, maintenance of its shape is important to interact with its environment for numerous functional aspects like cell signalling, motility, biofilm formation, etc. The cytoskeletal proteins play a crucial role in the determination of cell shape. Complex eukaryotic cells, as well as prokaryotes, possess different cytoskeletal proteins. In most non-spherical, cell-walled bacteria, MreB, which is a homolog of eukaryotic actin, coordinates with the peptidoglycan synthesis machinery for maintaining cell shape. Surprisingly, *Spiroplasma* is able to maintain a helical cell shape even in the absence of a cell wall. It has a unique cytoskeletal protein, Fibril and five MreB paralogs, out of which MreB5 was recently shown to be involved in attaining motility and helicity in a plant pathogen, *Spiroplasma citri*, indicating that the function of MreB paralogs might be non-redundant in this organism. The aim of my MS thesis work was to characterize *S.citri* MreB1, which is one of the five MreB paralogs. SUMO tag fusion-based approach was utilized for standardizing the purification of MreB1. The ATPase activity was quantified for all the different constructs of MreB1. CD spectroscopy confirmed the presence of secondary structures. Filaments were visualized using Transmission electron microscopy. In future, the project will focus on understanding the protein interaction with cell membrane and its partner proteins - Fibril and MreB paralogs. Further, it will pitch into designing ATPase mutants and polymerization mutants to understand filament dynamics and the possible role of nucleotides in the same.

Acknowledgement

I would like to thank my guide Dr Gayathri Pananghat for her constant support and guidance throughout my project tenure. She not only advised me regarding my thesis work but was also concerned about my well-being. I also thank Dr Sunish Radhakrishnan for the discussions and his valuable inputs for my project.

I extend my gratitude towards my mentor Mrinmayee for her care and support right from the very beginning of my project. I thank her for teaching me, helping me properly plan my experiments, and for her motivation and patience whenever I needed help. I thank Rinku for being a good mentor during my initial tough days in the lab and for all the help she provided. I also thank Apurba, Soumyajit, Sukanya and Rushik for their valuable suggestions and help with the purifications. I sincerely thank Suman and Anushka from JBU lab for their help with CD spectroscopy and mass spectrometry. I am also thankful to my batchmates Ranajana, Aishwarya and all the past and present G3 lab members for their support. I enjoyed working with all the ground floor lab members - SK lab, SKR lab and JBU lab. I thank Rushik and Mrinmayee again for all late night coffees and good food.

I am glad to have all my friends who never left my side in my good and bad times. I also thank my football team for making my life in IISER more thrilling, enjoyable and stress free. Lastly, I thank my family for their invaluable support and love.

Contributions

Contributor name	Contributor role
Dr. Gayathri Pananghat and Mrinmayee Bapat	Conceptualization Ideas
Dr. Gayathri Pananghat, Mrinmayee Bapat and Akhilesh Uthaman	Methodology
-	Software
Dr. Gayathri Pananghat	Validation
Dr. Gayathri Pananghat, Mrinmayee Bapat and Akhilesh Uthaman	Formal analysis
Akhilesh Uthaman	Investigation
Dr. Gayathri Pananghat	Resources
-	Data Curation
Akhilesh Uthaman	Writing - original draft preparation
Akhilesh Uthaman and Dr. Gayathri Pananghat	Writing - review and editing
-	Visualization
Dr. Gayathri Pananghat	Supervision
-	Project administration
Dr. Gayathri Pananghat	Funding acquisition

Chapter - 1
Introduction

1.1 Actin and its homologs

The cytoskeleton is a complex network of protein filaments which are crucial in cell shape maintenance of both prokaryotic and eukaryotic systems (Ridley et al., 2011). The eukaryotic cytoskeleton comprises actin filaments, intermediate filaments and microtubules. They perform numerous functions in eukaryotic cells, which mainly include cell motility, shape maintenance, cell division, anchorage of cellular organelles and intracellular transport (Pollard et al., 2009). Actin being the most abundant eukaryotic protein plays a major role in cell shape maintenance, cell polarity and regulation of transcription (Dominguez et al., 2011). Actin is also important in the formation of cell protrusions such as lamellipodia, filopodia, etc., thereby helping in functions such as cell migration (Pollard et al., 2009). Microtubules made of α-β tubulin dimers are required for intracellular transport, chromosome segregation, formation of cilia and flagella, etc., whereas intermediate filaments mainly provide mechanical support to cells.

Three decades back, it was believed that prokaryotes lacked cytoskeleton, but later it was found that they have tubulin homologs (de Boer et al., 1992) as well as actin homologs (Bork et al., 1992). FtsZ, TubZ, and BtubA-BtubB are some of the tubulin homologs identified in bacteria. TubZ is a component of the partitioning system which helps in the proper segregation of plasmids (important for low copy number plasmids) in some bacterial species (Berry et al., 2002). BtubA and BtubB show more sequence similarity to eukaryotic α-β tubulin and are thus believed to be acquired by horizontal gene transfer in some species which already have FtsZ (Sontag et al., 2009). FtsZ forms a z-ring in bacteria which in turn interacts with many other proteins for the advancement and execution of cell division (Margolin et al.,2005). CetZ is an example

of a tubulin homolog present in archaea. They form dynamic cytoplasmic filaments, which are thought to have possible membrane interactions, thereby having a role in determining cell shape (Wagstaff et al.,2018).

The homologs of actin known to date in bacteria are MreB, FtsA, ParM, MamK, etc. Crenactin is an actin homolog found in archaea. MreB is present in almost all non-spherical bacteria. MreB is predominantly responsible for the regulation of cell wall synthesis and in the regulation of the establishment of the elongasome complex (proteins required for cell elongation) (Szwedziak et al., 2013). FtsA is a cell division protein which is required for the anchorage of tubulin homolog FtsZ to the cell membrane (Wagstaff et al., 2018). ParM protein is part of a type II partition system called the ParMRC system, where ParR is a DNA binding protein, and *parC* is a centromeric region of DNA. ParR*C* complex recruits ParM filaments which in turn form a bipolar spindle required for proper segregation of plasmid DNA (Gayathri et al., 2012). MamK protein is found in magnetotactic bacteria where their role is in alignment and proper segregation of magnetosomes (komeili et al., 2006).

1.1.1 Protofilament and filament structures

The globular structure of actin is composed of four subdomains (IA, IB, IIA and IIB). Actin filaments are made of two filaments which are parallel and twisted. Longitudinal interaction of actin monomers results in filament formation. Higher-order structures are also favoured by these filaments for executing different functions (Wagstaff et al., 2018). ParM forms parallel double filaments, but ParM filaments show lefthandedness, unlike the actin filament, which has a right-handed twist (Orlova et al., 2007). FtsA does not have a usual actin fold but forms actin-like protofilaments (van den Ent et al., 2000). Even though domain IB is absent, an alternate domain 1C (Fig. 1.1 a) is formed as a result of insertion in domain IA. On lipid bilayers FtsA forms long doublets and other higher-order structures (Szwedziak et al., 2012). MamK also forms parallel, double and right-handed protofilaments similar to that of actin, but their monomers are juxtaposed, unlike actin and other homologs mentioned earlier (Löwe et al., 2016). Crenactin forms

double helical, parallel & staggered filaments which are right-handed (Izoré et al., 2016). MreBs have a distinct filament arrangement as they form antiparallel double straight filaments, unlike actin and most of its homologs (van den Ent et al., 2014).

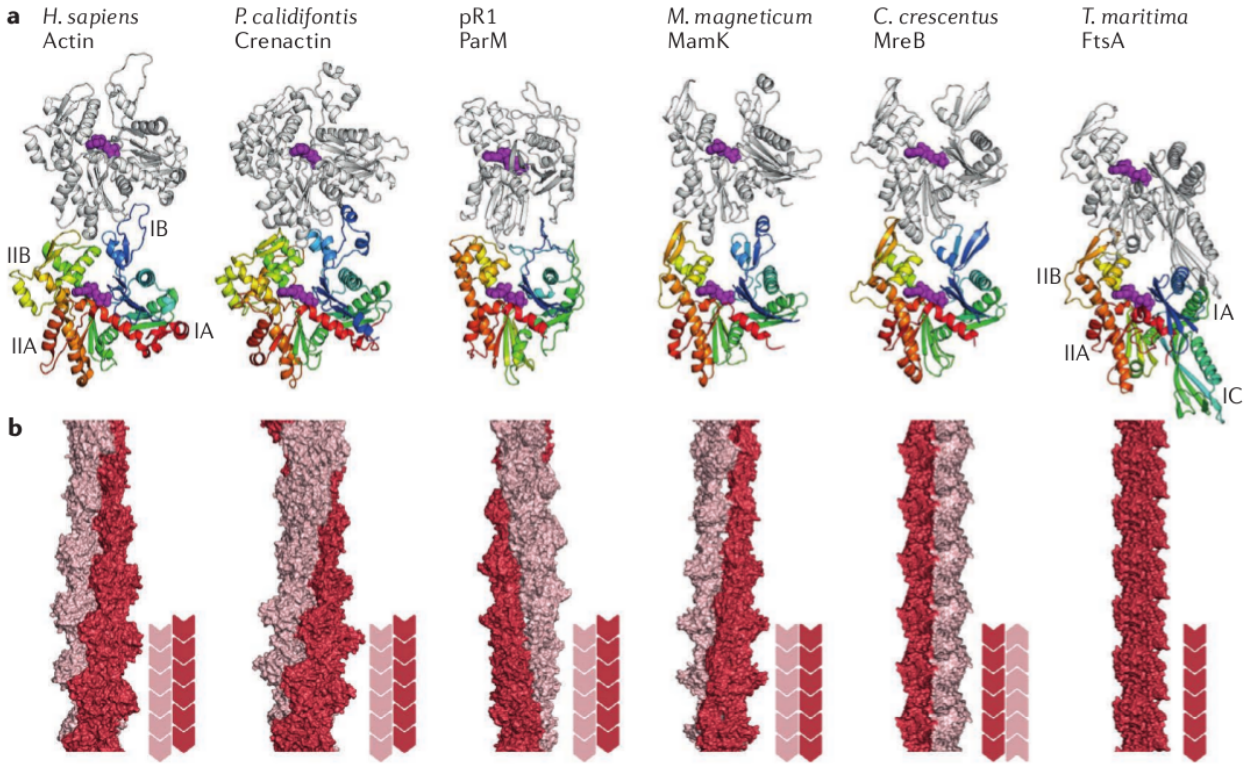

***Fig. 1.1*: Comparison of actin and its homologs.** (a) Monomer pairs of actin and different homologs. The lower subunit is coloured from blue (amino terminus) to red (carboxyl terminus). Nucleotide is coloured purple. (b) High-resolution structures of filaments obtained from cryo-electron microscopy or X-ray crystallography experiments. Filament polarity is represented by cartoon representation. (Adapted from *Wagstaff and Löwe, 2018*)

1.1.2 Active site and Polymerization

Actin monomers with bound ATP assemble on one another to form filaments. After polymerization, ATP gets rapidly hydrolyzed, but the release of γ-phosphate is slow. ADP-bound actin then dissociates from the filaments to recycle the subunits. Actin filaments undergo polymerization and depolymerization from both ends. The continuous addition of ATP bound actin at one end and the detachment of ADP bound actin from

the other end is termed treadmilling. At the plus/barbed end, polymerization is higher, whereas depolymerization is faster at the minus/pointed end (Chou et al., 2019). At a steady state, critical concentration is defined as the number of free monomeric actin present when the barbed end polymerization rate and the pointed end depolymerization rates are equal. Unlike actin, ParM filaments show dynamic instability (Garner et al., 2004), and this is thought to be crucial in its function of plasmid partitioning. Unless stabilized by the ParRC complex, the ParM filaments disassemble on their own, but if stabilized, they polymerize to segregate the plasmid (Garner et al., 2004). Residues from all four domains have contacts with the nucleotide, but most of the contacts are with the ribose and phosphate moieties, and this can be a reason why ParM is able to bind both ATP and GTP (Gayathri et al., 2013). ParM does not form filaments in the ADP state, unlike actin, as the critical concentration of ParM in the ADP bound-state is 100 times more than ATP-bound state (Garner et al., 2004). The critical concentrations of ATP and ADP bound states for ParM polymerization are 0.55 μM to 0.68 μM and ~ 100 μM, respectively (Garner et al., 2004).

In *Thermotoga maritima*, MreB (TmMreB) polymerization happens in the presence of either GTP or ATP. The critical concentration of the ATP state is 0.5 μM and the ADP state is 1.7 μM (Bean et al., 2008), and these are not very different from the critical concentration of actin (barbed end a - 0.12 μM and pointed end - 0.6 μM) (Pollard et al., 1986). This possibly rules out the chance of dynamic instability in MreBs. Unlike TmMreB, irrespective of the identity or presence of nucleotide, *Bacillus subtilis* MreB polymerizes with the same critical concentration of around 0.9 μM (Mayer et al., 2009). The difference in conditions of MreB polymerization across species might be an indication of a difference in function (Cabeen et al., 2010). Filaments are formed by MamK in the presence of ATP, but no filaments are observed in the presence of ADP. MamK also polymerizes in the presence of GTP but with a lower polymerization rate. The critical concentration of the ATP and GTP bound states are 0.69 ± 0.15 μM and 2.01 ± 0.23 μM (Ozyamak et al., 2013). FtsA forms linear ATP-dependent filaments *in vitro*. FtsZ filaments facilitate FtzA polymerization, and depolymerization of FtsZ facilitates the depolymerization of FtsA (Morrison et al., 2022).

1.2 MreB

Cell wall by itself is not sufficient in providing a particular shape to cells. In most non-spherical cell-walled bacteria, MreB is necessary for attaining this (van den Ent et al., 2010). In cell-walled bacteria, MreB is thought to work in coordination with the peptidoglycan synthesis machinery. MreB localizes in response to local cell shape cues and then recruits the cell wall synthesis machinery, bringing about the necessary changes. Thus, MreB localization is in a feedback loop with its function (Fig. 1.2) (Shi et al., 2018). Most of the gram-positive bacteria possess several paralogs of MreB, while most of the gram-negative bacteria have only a single copy of MreB. Also, in gram-negative bacteria, MreB binds to the cell membrane via an N-terminal amphipathic helix, whereas, in gram-positive bacteria, membrane binding is via a hydrophobic loop (Salje et al., 2011)(Maeda et al., 2012).

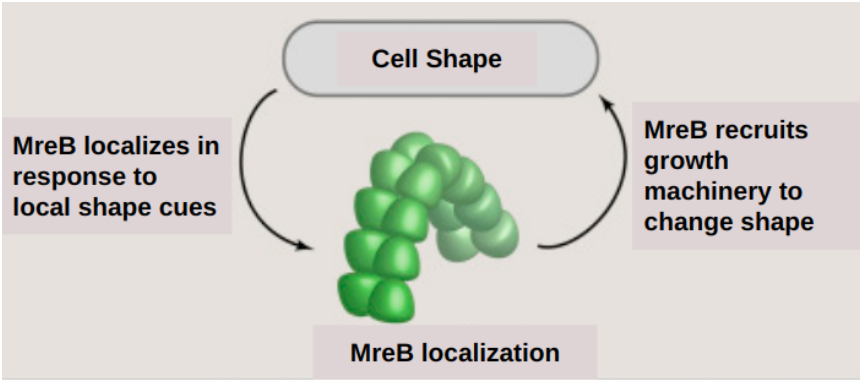

***Fig. 1.2*: A feedback loop exists for MreB function.** Schematic representation of the feedback loop between MreB localization and Cell shape maintenance. (Adapted from *Shi et al. Cell, 2018*).

It was observed that *E.coli* cells lost their rod shape in the absence of MreB. Restoration of rod shape is impossible in the absence of MreB (Kruse et al., 2005). In *E.coli*, different point mutations in the MreB gene were observed to be responsible for the loss of different attributes of cell shape (Shi et al., 2018). Fusion of YFP protein at the N-terminus of *E.coli* MreB resulted in non-functional MreB as the expression of MreB with N-terminal YFP fusion could only partially recover cell shape in MreB mutants (Swulius et al., 2012). This supports the finding that MreB binds to the membrane using

an N-terminal amphipathic helix in *E.coli* (van den Ent et al., 2014). In *Caulobacter crescentus,* the treatment with A22 (inhibitor of polymerization) leads to the eventual loss of native shape by the organism (Fig. 1.3). This proves that polymers of MreB have functional relevance (Gitai et al., 2005). The elongation of polar stalk of *C.crescentus* is MreB dependent. Unlike *E.coli,* which has only one homolog of MreB, *Bacillus subtilis* has three MreB paralogs: MreB, Mbl, MreBH. All of these show independent polymerization even if their co-localization is important for cell shape maintenance (Dempwolff et al., 2011). When expressed all together or co-expressed in different pair-wise combinations in *E.coli*, their filament architecture seems to be influenced by each other and colocalize together. It is still not clear whether they co-polymerize and form a bundle or whether single filaments of each type come together to form a mixed bundle. MreB mutants in *B.subtilis* become wider and form bulges at the site of division. Mbl mutants form twisted and bent cells. MreBH mutants show normal growth under usual conditions but seem necessary for growth under low Mg^{2+} conditions (Soufo et al., 2010). Also, during phage infection in *B.subtilis,* phage DNA localization is MreB dependent (Muñoz-Espín et al., 2009). In *Helicobacter pylori*, the deletion of MreB surprisingly does not alter the shape or affect viability but reduces the level of urease (urease is important in the colonization of these bacteria). Also, since MreB was detected as one of the antigens in patients suffering from gastric cancer, it was proposed to have a role in pathogenicity (Gurrola et al., 2017). In *Pseudomonas aeruginosa,* MreB has a role in pilus-driven motility

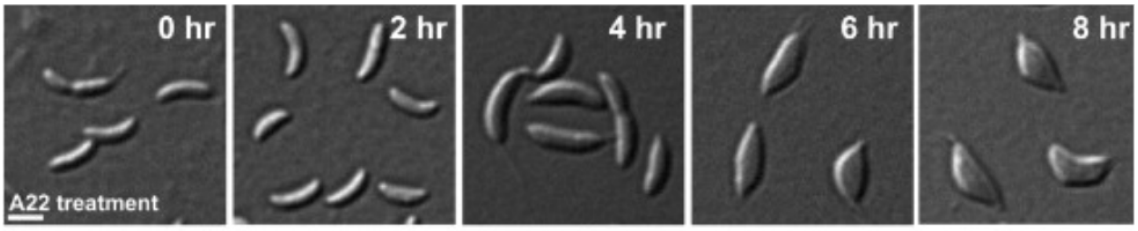

***Fig. 1.3*: A22 changes *Caulobacter* morphology.** *Caulobacter* grown in the presence of 10 µg/ml A22 for 8 hours (Adapted from *Gitai, Zemer et al. Cell, 2005*)

Even though MreB seems to have more than one function, the vital function out of all those is still cell shape maintenance. In cell-walled bacteria, MreB functions in

coordination with peptidoglycan synthesis machinery. Strikingly, there are cell wall-less bacteria as well, which are still able to maintain a particular shape. Helical-shaped *Spiroplasma*, *Haloplasma* etc., are examples for these. In these bacterial species as well, the presence of MreBs are confirmed. It will be interesting to study how MreBs function in these organisms to achieve this function of cell-shape maintenance.

1.3 Spiroplasma

Spiroplasma belongs to the class of Mollicutes. The most intriguing feature of *Spiroplasma* is that they are able to maintain a helical cell shape even if they lack a cell wall (Razin et al., 1973). Even in the absence of appendages, they are motile and chemotactically active (Daniels et al., 1980). They show twitching, flexing and rotation along their helical axis (Kürner et al., 2005). They move by the propagation of kinks. Swapping the handedness of the helix is involved in swimming through propagation of kinks, but the mechanism of how they do this is unknown (Sasajima et al., 2021). Cell division in *Spiroplasma* is thought to happen in two ways: One along the short axis (cross-sectional) (Garnier et al., 1981) and the other one along the long axis (Y-shaped), in which the latter is observed in *S.poulsonii* (Ramond et al., 2016). It is still not clear how *Spiroplasma* is able to maintain its shape. With the help of cryo-electron tomography, it was shown that two types of filaments (thick and thin in width based on interfilament spacing), which are arranged parallelly, form three ribbons which span from one end to the other in *Spiroplasma melliferum* (Kürner et al., 2005). The thickness of isolated filaments showed that the two outer ribbons were made of Fibil (Fib) protein, a cytoskeleton protein specific to *Spiroplasma* species. Whole genome sequencing confirmed the presence of five homologs of MreB in *Spiroplasma citri*. Comparing filament thickness obtained from tomogram and the thickness of already characterized *Thermotoga maritima* MreB, it was proposed that the inner ribbon is made of MreB filaments. Also, from the western blot and sequence alignment, the presence of MreB and fibril in *S.melliferum* was confirmed again (Kürner et al., 2005). From electron tomography, Fib filaments were found lying in close contact with the cell membrane (Kürner et al., 2005). Fib is therefore thought to play a important role in the helical

shape maintenance. Even though the relevance of multiple MreB homologs is still questionable, *Spiroplasma* has five or more MreB genes which possibly provide the organism with a selective advantage (Harne et al., 2020).

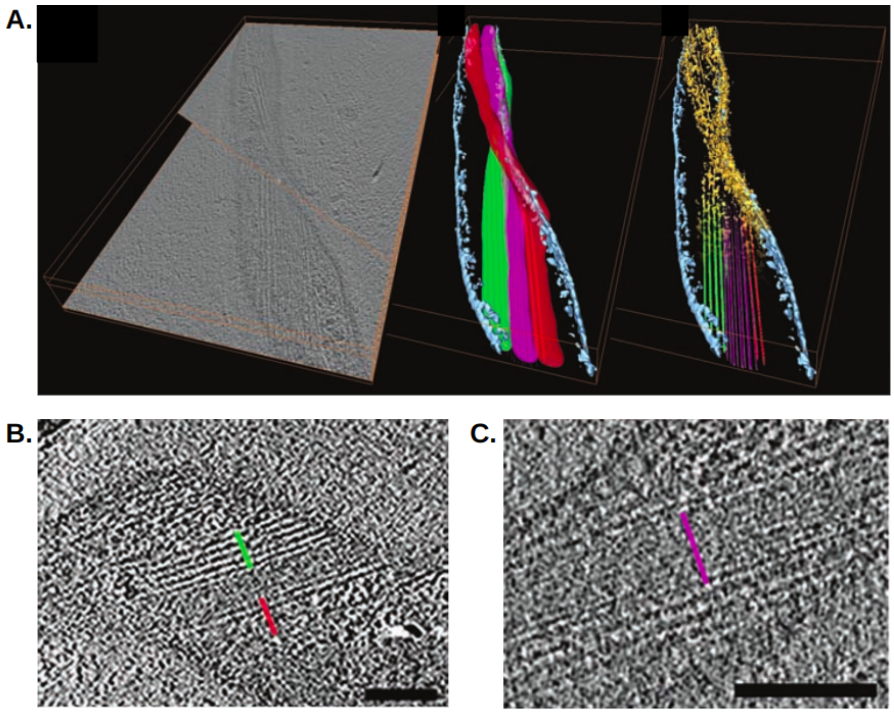

***Fig. 1.4*: Cryo-Electron Tomography discloses the presence of a cytoskeletal ribbon made of Fibril and MreBs.** (A) Superimposed slices from various Z heights of cryo-electron tomogram (left-most image) and 3D visualization (middle and right-most images) in which red and green are the outer ribbons made of fibril (B) Red and green correspond to thicker filaments - 11 nm spacing (C) Thinner filaments - 4 nm spacing. (Adapted from *Kurner et al. Science, 2005*)

Recently, a study was done using a *mycoplasma-based* minimal cell (syn3B) and synthetically designed genome, which had five *Spiroplasma eriocheiris* MreB genes and the Fib gene encoded (Kiyama et al., 2022). They observed the phenotype of shape and motility after the depletion of each of these single genes, the phenotype when only one of these genes is present and the phenotype when more than one genes are present together in different combinations. The combination of MreB5-MreB1 and MreB5-MreB4 resulted in helicity and motility. Filamentous morphology was seen in some combinations. The combination of MreB3-MreB1, MreB3-MreB4 and

MreB3-MreB5 remained spherical (Fig. 1.5). Even without Fib, the cell was showing helicity and motility. So, the direct role of Fib in these is ambiguous (Kiyama et al., 2022). Another similar study was done where all five MreBs and Fib of *S.citri* were heterologously expressed in *Mycoplasma capricolum* (Lartigue et al., 2022). The expression of these proteins shifted morphology from a spherical to an elongated shape. Apart from this, the expression also endowed the cell with helicity and kinking motility. Expression of Fib, MreB5 or MreB1 resulted in helicity, and when both MreB1 and Fib were co-expressed, the helices became tight. The mean pitch observed was similar to *Spiroplasma* only when MreB5 was expressed. MreB1, MreB5 and Fib were thought as the minimal requirement for inducing helicity in cell wall-less bacteria. For kinking motility, MreB5 was shown to be the minimal requirement, even if the role might not be direct (Lartigue et al., 2022).

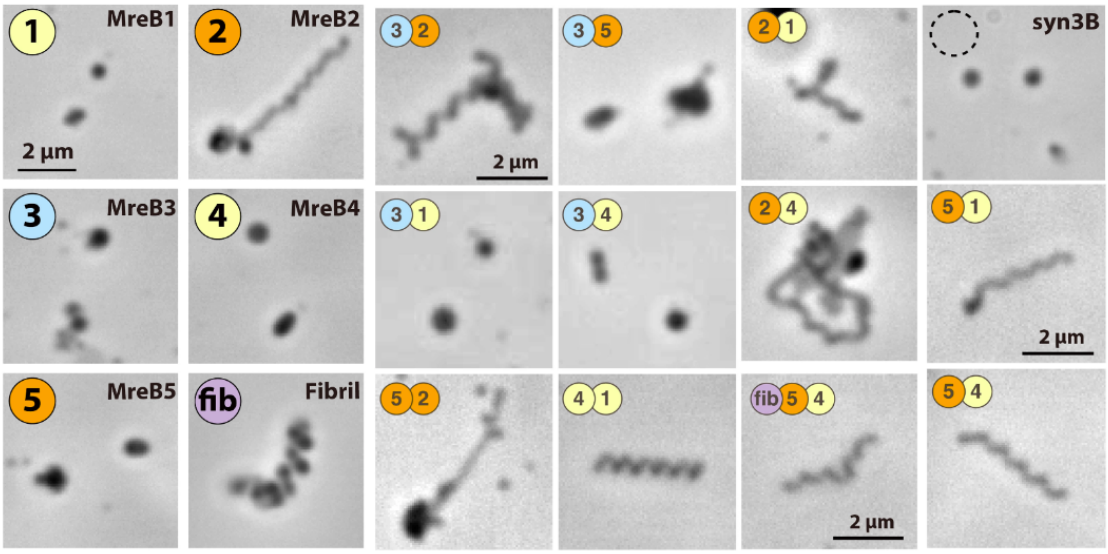

***Fig. 1.5*: Expression of Fibril and different MreBs impart helicity and motility to synthetic minimal cell.** Phase-contrast image of syn3B minimal cell morphology pre and post-expression of MreBs or Fibril individually or in combinations (Adapted from *Kiyama, Hana et al. Science Advances, 2022*)

1.4 *Spiroplasma citri* MreBs and Fibril

The model organism that we are interested in is *Spiroplasma citri*. *S.citri* is known to cause “Citrus stubborn disease” in citrus plants. This has five paralogs of MreB and a fibril cytoskeleton protein. Whole genome sequencing of the non-helical, non-motile natural variant of *S.citri*, ASP-I, had shown that there was a point mutation in the MreB5 gene, as a result of which it forms truncated MreB5 spanning 133 amino acids instead of 352 amino acids (Harne et al., 2020). All the other MreBs and Fibril protein was found to be unaffected. To check whether MreB5 had any role in the loss of helicity and motility in ASP-I, wild-type MreB5 was expressed using a vector-based approach under the *tuf* promoter. The expression of wild-type MreB5 changed the ASP-I phenotype similar to that of wild-type *S.citri*. Based on this, it was concluded that MreB5 is important in maintaining helicity and motility. Also, this was a sign that at least some of the MreBs might be having a specific, non-redundant function in shape determination. Also, in vitro sedimentation (co-pelleting) assay was done to prove that *S.citri* MreB5 (ScM5) interacts with Fib. This was possible because Fib always came in pellet fraction when spun at high speed (159000 g), and at this speed, ScM5 remained only in the supernatant. When both were mixed and then spun at 159000 g, then ScM5 also came in pellet fraction, and the amount of ScM5 in pellet showed an increase with an increase in Fib concentration (Fig. 1.6) (Harne et al., 2020). Similar to this, co-pelleting assay was done for MreB and liposomes. In this as well, MreB5 pelleted along with liposomes suggesting possible interaction of MreB5 with the cell membrane (Harne et al., 2020).

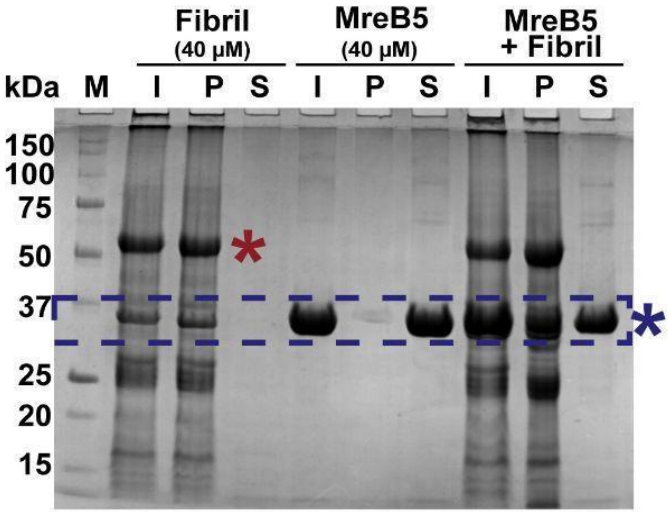

***Fig. 1.6*: Co-pelleting assay reveals ScM5-Fib interaction.** SDS PAGE gel image for the co-pelleting assay of *S.citri* Fib and MreB5. MreB5 comes in pellet fraction only in the presence of Fib. (Adapted from *Harne et al. Current Biology, 2020*)

1.5 SUMO tag as a strategy for protein solubilization and purification

Our lab works on the characterization of *S.citri* MreBs and Fib. Out of the five MreBs, ScM5 is already characterized in our lab. Work on *S.citri* MreB1 (ScM1) has been initiated. The construct which was used initially for the characterization of ScM1 was pHis17_M1_$(His)_6$ (*S.citri* MreB1 with a hexa histidine tag at the C terminus). The protein expressed well in BL21AI strain, but the solubility was only around 60 to 70 %. Also, the protein was not that stable, as of result of which it precipitates. Therefore the total yield of protein obtained after purification was always in very less amounts. After size exclusion chromatography, the majority of the protein comes in void and the peak is spread from void to monomer. To take this forward, the primary focus was on increasing the solubility of the protein. To achieve this, it was decided to clone a construct with a SUMO tag at the N-terminus of the protein.

SUMO stands for Small Ubiquitin-like Modifier. It plays an important role in protein transport regulation, transcription control, stress response, etc. in eukaryotes. SUMO tag enhances protein folding and stability when it is used as an N-terminal fusion protein (Young et al., 2012). It improves protein solubility and yield by increasing expression

and reducing degradation. For the purification of SUMO-tagged proteins, an additional histidine tag is usually preferred as there are no columns with specificity to the SUMO tag. Another benefit of the SUMO tag is that after purification of the SUMO-tagged protein, the tag can be specifically removed via a protease-based cleavage, thereby resulting in a native, untagged protein. Ulp1 protease (*Saccharomyces cerevisiae*) cleaves after the Gly-Gly motif at the C-terminus of the SUMO tag, and the cleavage is very specific. The recognition by the SUMO protease (Ulp1) is not based on the amino acid sequence but on the tertiary structure (Young et al., 2012).

1.6 Objectives:

The main aim of my MS thesis project is to characterize *Spiroplasma citri* MreB1 (ScM1). To achieve this, the following objectives were proposed:

[1] Cloning, overexpression and purification of ScM1
[2] Thermal shift assay to analyse the stability of ScM1
[3] Malachite green assay to quantify ATPase activity of ScM1
[4] Pelleting assay for monitoring polymerization of ScM1
[5] CD spectroscopy for secondary structure estimation of ScM1
[6] Transmission Electron Microscopy to see filament formation, if any, by ScM1

Different constructs were designed for this which includes $(His)_6$-SUMO-M1, ATPase mutant $(His)_6$-SUMO-M1 - E137A, $(His)_6$-SUMO-M1-Strep, and $(His)_6$-SUMO-M1-Strep - E137A. The biochemical and functional characterization as listed above was attempted for all the four constructs.

Chapter - 2
Materials and Methods

2.1 Cloning

Cloning of all the different constructs used were PCR based, with restriction free (RF) cloning as the main strategy.

2.1.1 PCR

Polymerase Chain Reaction (PCR) was used for cloning purposes. PCR components comprise primers, template, deoxynucleotide triphosphates (dNTPs) and polymerase. Primers were designed and ordered from BioServe Biotechnologies (India) Pvt.Ltd. dNTP mix (10 mM each of dATP, dCTP, dTTP & dGTP) were ordered from Puregene / Nirav BioSolutions. The polymerase used was Pfu polymerase (*Pyrococcus furiosus* polymerase; purified in-house).

2.1.2 Restriction Free cloning

For the purpose of cloning different constructs, restriction free (RF) cloning method was used. This consists of two rounds of PCR. In the first PCR (PCR 1), the gene of interest is amplified with overhangs having overlap to the flanking regions of vector at 5' and 3' ends. The amplified product from PCR 1 was subjected to PCR purification using Qiagen PCR purification kit. This purified product (mega primer) was used for the incorporation of the gene in the vector using the restriction free method (PCR 2). Both test (T, reaction with both template and insert) and control (C, reaction with only template) were kept for PCR 2. Also, five microlitres were kept aside separately from both the test and control without subjecting to PCR (T_o and C_o, respectively), and all four reactions (T, C, T_0 and C_o) were ran on an 0.8% agarose gel to check whether PCR 2 gave rise to a higher band upon incorporation of the megaprimer into the plasmid. Both T and C were then treated with DpnI (0.5 µL of DpnI added to 9.5 µL of T and C) and

kept for incubation at 37 ^{O}C for 3 to 4 hours. After incubation, these DpnI-treated T and C were transformed into NEB Turbo electrocompetent cells via electroporation. Post transformation, the cells were plated on antibiotic-resistant Luria Bertani (LB) agar plates (if kanamycin: 25 mg/ml; if ampicillin: 50 mg/ml). These plates were incubated for around 12 to 16 hours at 37 ^{O}C. Few single colonies (around 5 to 7) were separately inoculated in 10 ml LB broth media and incubated at 37 ^{O}C overnight. These cultures were pelleted post-incubation, and plasmids were isolated from pellets by following Qiagen plasmid purification protocol using the kit. A gene amplification PCR was done as a preliminary clone check method using gene-specific forward and reverse primers and these isolated plasmids as templates. All the positive clones from the above clone check PCR were then subjected to double digestion (restriction digestion with enzymes which have restriction sites next to the gene) check. Each reaction of this had 0.5 µL each of both the enzymes, 1 µL of 10x CutSmart buffer, ~ 150 ng of plasmid and the rest of it Milli-Q water. Clones which gave expected release lengths were sent for sequencing.

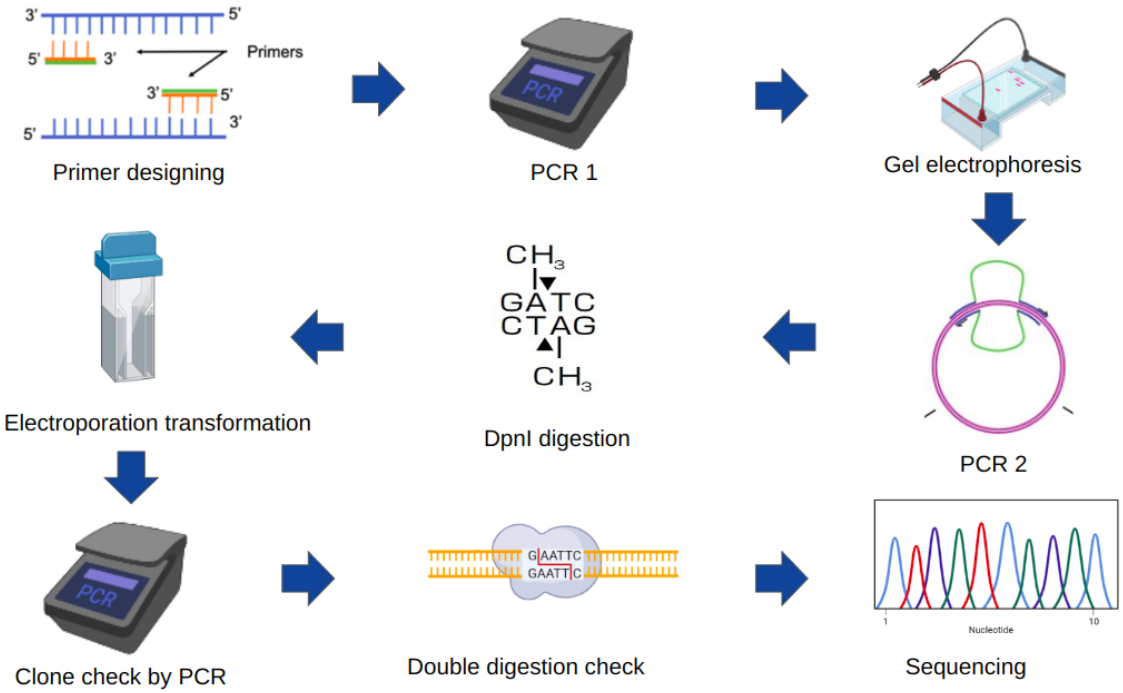

Fig. 2.1: **Flowchart of RF cloning.** Schematic showing workflow of RF cloning from primer designing to sequencing (*created with BioRender.com*)

Table 2.1 Set of primers

Construct	Primers (5' to 3')
$(His)_6$-SUMO-M1	Forward primer: CCGCGAACAGATTGGTGGCCATATGGCCATATTTAATAATAAGAAGCC Reverse Primer: CGACGGAGCTCGAATTCGGATCCTTAATAATCTAATTCTTTTGTTTTATG
$(His)_6$-SUMO-M1-E137A	Forward primer: GTTTTTGTTGAAGAAGCGGTTAAAATGGCTGC Reverse Primer: CGACGGAGCTCGAATTCGGATCCTTAATAATCTAATTCTTTTGTTTTATG
$(His)_6$-SUMO-M1-Strep	Forward primer: CCGCGAACAGATTGGTGGCCATATGGCCATATTTAATAATAAGAAGCC Reverse Primer 1: CGAACTGAGGATGAGACCAGGATCCATAATCTAATTCTTTTGTTTTATG Reverse Primer 2: CGACGGAGCTCGAATTCGGATCCTTATTTTTCGAACTGAGGATGAGACC
$(His)_6$-SUMO-M1-Strep-E137A	Forward primer: GTTTTTGTTGAAGAAGCGGTTAAAATGGCTGC Reverse Primer: CGACGGAGCTCGAATTCGGATCCTTATTTTTCGAACTGAGGATGAGACC

Note: Sequence in red corresponds to pET28a vector, blue corresponds to ScM1 gene and green corresponds to strep-tag, The codon highlighted in yellow represents the mutation. CATATG (underlined) is the NdeI restriction site and GGATCC (underlined) is the BamHI restriction site.

Details of different constructs used for the characterization of ScM1 are given below:

- $(His)_6$-SUMO-M1 (50.5 kDa) ScM1 (38.1 kDa) with a SUMO tag (11.1 kDa) at the N-terminus followed by a hexa-histidine tag (0.8 kDa) at the N-terminus of SUMO tag

- $(His)_6$-SUMO-M1 - E137A (50.4 kDa) $(His)_6$-SUMO-M1 with a point mutation (E137A) in the ScM1 gene
- $(His)_6$-SUMO-M1-Strep (51.7 kDa) $(His)_6$-SUMO-M1 with an extra Strep tag (1.1 kDa) at the C-terminus of ScM1
- $(His)_6$-SUMO-M1-Strep - E137A (51.6 kDa) $(His)_6$-SUMO-M1-Strep with a point mutation (E137A) in the ScM1 gene

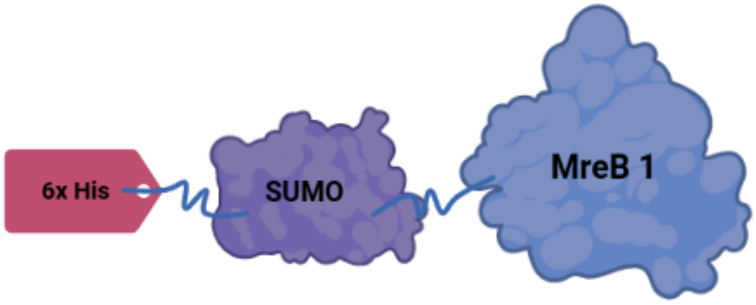

Fig. 2.2: **Pictorial representation of $(His)_6$-SUMO-M1.** ScMreB1 with SUMO tag at the N-terminus followed by a hexahistidine tag at the N-terminus of SUMO tag (*created with BioRender.com*)

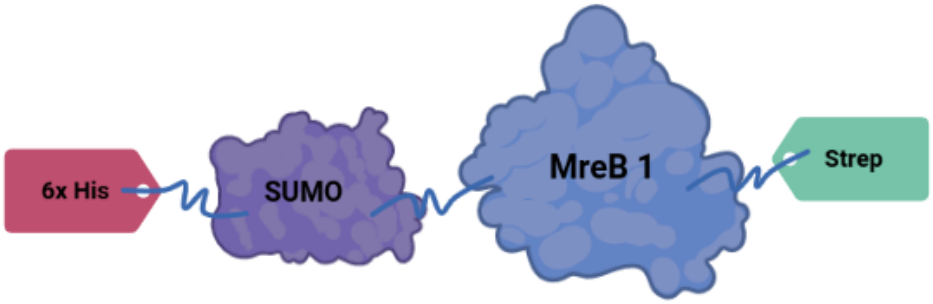

Fig. 2.3: **Pictorial representation of $(His)_6$-SUMO-M1-Strep.** ScMreB1 with Strep tag at the C-terminus, SUMO tag at the N-terminus followed by a hexahistidine tag at the N-terminus of SUMO tag (*created with* BioRender.com)

Table 2.2 : PCR 1 components for the cloning of $(His)_6$-SUMO-M1

Components	Reaction 1	Reaction 2
Template (pHis17_M1) - 152 ng/µL	1 µL	1 µL
Forward primer (20 µM)	1 µL	1 µL
Reverse primer (20 µM)	1 µL	1 µL
10x Pfu Buffer	5 µL	5 µL
Pfu Polymerase	1 µL	1 µL
2.5 mM dNTPs	2 µL	2 µL
Milli-Q	39 µL	39 µL

Table 2.3 : PCR 2 components for the cloning of $(His)_6$-SUMO-M1

Components	Test	Control
Template (pET28a_FtsA) - 490 ng/µL	1 µL	1 µL
Insert - 200 ng/µL	8 µL	-
10x Pfu Buffer	5 µL	5 µL
Pfu Polymerase	1 µL	1 µL
2.5 mM dNTPs	4 µL	4 µL
Milli-Q	31 µL	39 µL

Table 2.4 : PCR 1 and PCR 2 conditions for the cloning of $(His)_6$-SUMO-M1

Step	PCR 1		PCR 2	
	Temperature (^{O}C)	Time	Temperature (^{O}C)	Time
Initial Denaturation	95	5 min	95	5 min
Denaturation	95	30 sec	95	30 sec
Annealing	58	35 sec	55	50 sec
Extension	72	70 sec	72	6.42 min
Final Extension	72	10 min	72	10 min
Hold	4	-	4	-

Table 2.5 : PCR 1 components for the cloning of $(His)_6$-SUMO-M1 - E137A

Components	Reaction 1	Reaction 2
Template (pET28a_$(His)_6$-SUMO-M1) - 252 ng/µL	0.5 µL	0.5 µL
Forward primer (20 µM)	1 µL	1 µL
Reverse primer (20 µM)	1 µL	1 µL
10x Pfu Buffer	5 µL	5 µL
Pfu Polymerase	1 µL	1 µL
2.5 mM dNTPs	2 µL	2 µL
Milli-Q	39.5 µL	39.5 µL

Table 2.6 : PCR 2 components for the cloning of $(His)_6$-SUMO-M1 - E137A

Components	Test	Control
Template (pET28a_$(His)_6$-SUMO-M1) - 252 ng/µL	1.5 µL	1.5 µL
Insert - 208 ng/µL	7 µL	-
10x Pfu Buffer	5 µL	5 µL
Pfu Polymerase	1 µL	1 µL
2.5 mM dNTPs	4 µL	4 µL
Milli-Q	31.5 µL	38.5 µL

Table 2.7 : PCR 1 (Step-1) components for the cloning of $(His)_6$-SUMO-M1-Strep

Components	Reaction 1	Reaction 2
Template (pET28a_$(His)_6$-SUMO-M1) - 252 ng/µL	1 µL	1 µL
Forward primer (20 µM)	1 µL	1 µL
Reverse primer (20 µM)	1 µL	1 µL
10x Pfu Buffer	5 µL	5 µL
Pfu Polymerase	0.7 µL	0.7 µL
2.5 mM dNTPs	2 µL	2 µL
Milli-Q	39.3 µL	39.3 µL

Table 2.8 : PCR 1 (Extension step) components for the cloning of $(His)_6$-SUMO-M1-Strep

Components	Reaction 1	Reaction 2
Template (Step-1 product) - 129 ng/µL	3 µL	3 µL
Forward primer (20 µM)	1 µL	1 µL
Reverse primer (20 µM)	1 µL	1 µL
10x Pfu Buffer	5 µL	5 µL
Pfu Polymerase	0.7 µL	0.7 µL
2.5 mM dNTPs	2 µL	2 µL
Milli-Q	37.3 µL	37.3 µL

Table 2.9 : PCR 2 components for the cloning of $(His)_6$-SUMO-M1-Strep

Components	Test	Control
Template (pET28a_$(His)_6$-SUMO-FtsZ) - 250 ng/µL	1.6 µL	1.6 µL
Insert (PCR 1 final product) - 129 ng/µL	9 µL	-
10x Pfu Buffer	5 µL	5 µL
Pfu Polymerase	0.8 µL	0.8 µL
2.5 mM dNTPs	4.5 µL	4.5 µL
Milli-Q	29.1 µL	38.1 µL

Table 2.10 : PCR 1 and PCR 2 conditions for the cloning of $(His)_6$-SUMO-M1-Strep

Step	PCR 1 (Both the steps)		PCR 2	
	Temperature (^{O}C)	Time	Temperature (^{O}C)	Time
Initial Denaturation	95	5 min	95	5 min
Denaturation	95	30 sec	95	30 sec
Annealing	60	35 sec	55	50 sec
Extension	72	120 sec	72	8 min
Final Extension	72	10 min	72	10 min
Hold	4	-	4	-

Table 2.11 : PCR 1 components for the cloning of $(His)_6$ -SUMO-M1-Strep - E137A

Components	Reaction 1	Reaction 2
Template (pET28a_$(His)_6$-SUMO-M1-Strep) - 447 ng/µL	0.5 µL	0.5 µL
Forward primer (20 µM)	1 µL	1 µL
Reverse primer (20 µM)	1 µL	1 µL
10x Pfu Buffer	5 µL	5 µL
Pfu Polymerase	1 µL	1 µL
2.5 mM dNTPs	2 µL	2 µL
Milli-Q	39.5 µL	39.5 µL

Table 2.12 : PCR 2 components for the cloning of $(His)_6$ -SUMO-M1-Strep - E137A

Components	Test	Control
Template (pET28a_$(His)_6$-SUMO-M1-Strep) - 447 ng/µL	1 µL	1 µL
Insert (PCR 1 final product) - 283 ng/µL	4.5 µL	-
10x Pfu Buffer	5 µL	5 µL
Pfu Polymerase	1 µL	1 µL
2.5 mM dNTPs	3.5 µL	3.5 µL
Milli-Q	35 µL	39.5 µL

Table 2.13 : PCR 1 and PCR 2 conditions for the cloning of $(His)_6$ -SUMO-M1-Strep - E137A

Step	PCR 1 (Both the steps)		PCR 2	
	Temperature (^oC)	Time	Temperature (^oC)	Time
Initial Denaturation	95	5 min	95	5 min
Denaturation	95	30 sec	95	30 sec
Annealing	59	35 sec	55	50 sec
Extension	72	1 min	72	8 min
Final Extension	72	10 min	72	10 min
Hold	4	-	4	-

2.2 Expression check

Expression check of all different constructs were done in BL21AI and Rosetta-DE3. After obtaining induced culture pellet, the protocol followed for expression check was same irrespective of the strain or the identity of the construct**.**

2.2.1 Expression strains

BL21AI:

BL21AI is a chemically competent *E.coli* expression strain. This was used for the expression of different constructs of *S.citri* MreB1. Around 200 nanograms of desired plasmid were used for heat shock transformation. The antibiotic plate with transformed cells were left in the incubator for 12 to 16 hours at 37 ^{O}C. 0.2% L-arabinose was used for induction of protein expression along with other vector specific inducer, if any.

Rosetta (DE3):

Rosetta-DE3 is a derivative of BL21AI used for expression of proteins with codons used sparsely in *E.coli*. This was used for expression of various *S.citri* MreB1 constructs. Around 200 nanograms of vector were used for transformation via heat shock. Chloramphenicol (25 mg/ml) was added along with other antibiotics in LB agar plate as the tRNA genes corresponding to those rare codons are present on a chloramphenicol resistant plasmid. Post transformation plates were left in the incubator at 37 ^{O}C for 12 to 16 hours.

2.2.2 Expression check protocol

Plasmids containing the gene of interest was transformed into desired expression strain. From the plate, a patch of colonies are transferred into 10 ml LB media with antibiotic in a test tube. This culture was grown at 37 ^{O}C until optical density (OD) reached 0.6. From this 10 ml culture, 5 ml was transferred to another test tube. This 5 ml culture was induced with respective inducers. Both induced and uninduced cultures were incubated for around 12 to 16 hours at 18 ^{O}C. After induction, cultures were pelleted. Both induced

and uninduced pellets were then resuspended in 500 µL lysis buffer (300 mM KCl, 50 mM Tris pH 8, 10% glycerol). After that, these were subjected to sonication (Vibra-Cell Ultrasonic Liquid Processors) using a small probe (1 second ON, 3 seconds OFF, for 1 minute). Post sonication 10 µL from induced and uninduced was mixed with 10 µL of 2x SDS loading dye (these two fractions were named as induced total and uninduced total to indicate the total cell lysate). Rest of the uninduced and induced were spun at 15000 r.p.m at 4 ^{O}C for 10 minutes in a table top centrifuge. After spin was over, 10 µL from the supernatant of both induced and uninduced were mixed with 10 µL of 2x SDS loading dye (these two fractions were named induced supernatant and uninduced supernatant, to indicate the soluble fraction of the cell lysate). All four SDS gel samples (induced total, uninduced total, induced supernatant and uninduced supernatant) were heated for 10 minutes at 99 ^{O}C and then ran on a 12% SDS gel at 230 V. After imaging the gel, protein expression and solubility were analyzed.

2.3 Protein purification

Purification techniques used were Ni-NTA affinity chromatography, Strep affinity chromatography and size exclusion chromatography (gel filtration).

2.3.1 Ni-NTA affinity chromatography

The culture pellet was resuspended in lysis buffer (around 30 - 40 ml of lysis buffer for 1L pellet) and then transferred to a rinsed beaker. This was subjected to sonication (1 second ON, 3 seconds OFF, for 3 minutes, followed by 5 minutes break and again a cycle of sonication). After sonication 10 µL of the lysate was mixed with 10 µL of 2x SDS loading dye and kept aside as total cell lysate fraction. Total cell lysate was spun in Beckman Coulter high-speed centrifuge (JA 25.50 Rotor) for 50 minutes at 4 ^{O}C at 15000 r.p.m. 5 ml HisTrap HP (Cytiva) His tag protein purification column was kept equilibriated with binding buffer (Buffer A) for proper binding of His-tagged protein to nickel. Following centrifugation of the total lysate, the supernatant was collected and loaded onto the equilibrated HisTrap column at a flow rate of 2 to 2.5 ml/minute. Flow

through was collected in a flask. After this, one round of 50 ml buffer A wash was given to remove other non-specifically bound proteins, which was collected as wash. Consequently, 50-60 ml of 2% and 5% buffer B (for example, 5% buffer B refers to 5% of buffer B and 95% of buffer A) wash was given. This was also collected in separate conical flasks. Then, 25 ml (i.e., five fractions of 5 ml each) each of 10%, 20%, 50% and 100% buffer B wash was given. During this elution, each 5 ml was collected in separate test tubes. After this, 10 µL from all the different collected fractions (total lysate, supernatant, flow through, wash, 2%, 5%, 10%, 20%, 50% and 100%) were ran on a 12% SDS gel. Based on the gel, the eluted fractions to be pooled for dialysis were identified based on the purity of the protein in the fractions. The pooled fractions were dialysed against 2L of buffer A to remove imidazole. After this, the protein was concentrated using 10 KDa Sartorius Vivaspin Turbo centricons (5000 r.p.m, 4 ^{O}C), made 10 µL aliquots, flash freezed using liquid nitrogen and stored at -80 ^{O}C. After use, the column was washed with an excess of 100 % buffer B and then with Milli-Q water.

Table 2.14 Purification buffers and their composition

Buffers	Composition
Lysis buffer	300 mM KCl, 50 mM Tris pH 8, 10% Glycerol
Buffer A (Binding buffer)	300 mM KCl, 50 mM Tris pH 8
Buffer B (Elution buffer)	300 mM KCl, 50 mM Tris pH 8, 500 mM imidazole
Dialysis buffer	300 mM KCl, 50 mM Tris pH 8
Strep-tag binding buffer	300 mM KCl, 50 mM Tris pH 8
Size exclusion chromatography buffer	300 mM KCl, 50 mM Tris Tris pH 8

2.3.2 Strep-tag affinity chromatography

Strep 5 ml StrepTrap HP column (Cytiva) was kept equilibriated with strep-tag binding buffer (refer Table 2.14) prior to the loading of Ni-NTA chromatography eluted fractions post dialysis. While loading, flow through was collected in a conical flask. After loading, a 50 ml wash was given with the same strep-tag binding buffer, and this was collected as wash. 2.5 mM of D-desthiobiotin (Merck Millipore) was used for elution of bound proteins. 2.5 mM D-desthiobiotin was prepared by dissolving 8 mg of D-desthiobiotin powder in 15 ml strep-tag binding buffer and was filtered before use. Elution was done by two rounds of 5 ml D-desthiobiotin injection. A total of 24 ml was collected in twelve 2 ml microcentrifuge tubes during elution. 10 µL from all different fractions (flow through, wash and 12 elution fractions) were checked on a 12% SDS gel. Post gel analysis, fractions containing pure protein were identified and concentrated using 10 KDa Sartorius Vivaspin Turbo centricons (5000 r.p.m, 4 ^{O}C). 10 µL aliquots were made from concentrated protein, flash freezed and stored at -80 ^{O}C. After use, column was washed by injecting 0.5 M NaOH and then excess Milli-Q wash was given before disconnecting.

2.3.3 Size exclusion chromatography

After Ni-NTA affinity chromatography, protein was concentrated to less than 1 ml in volume. Before loading the concentrated protein, size exclusion column (Biorad ENrich SEC 650 10 x 300 mm 24 ml size exclusion column) was equilibriated with equilibriation buffer. Once equilibriation was done, protein was injected using a 1 ml syringe. After loading, protein was eluted and collected as 1 ml fractions at a flow rate of 0.3 - 0.4 ml/minute. From the elution profile, the fractions corresponding to the peak (based on the profile by monitoring at 280 nm absorbance) were checked on SDS PAGE. Based on the gel, essential fractions were pooled and concentrated. After use, column was washed with excess of milli-Q.

2.3.4 Bradford assay for protein concentration estimation

Concentration of protein was estimated using Bradford assay. BSA (bovine serum albumin) of concentrations ranging from 0.1 to 1 mg/ml were kept as standards. 5 µL of each of the different BSA standards (0.1, 0.2, 0.3, …..,0.9, 1 mg/ml) were added in a 96 well plate (Tarsons skirted 96 well 0.2 ml plate). Also 5 µL of buffer was added in another well as buffer blank. 250 µL of Bradford reagent (Biorad Quick Start Bradford 1x Dye Reagent) was added to all these wells. Absorbance was measured at 595 nm using CLARIOstar Plus multimode microplate reader (BMG LABTECH). From the absorbance values of standards, the absorbance value of buffer blank was subtracted and then plotted against concentration of these standards. From the slope of the graph, the concentration of the protein was estimated.

2.3.5 SUMO tag cleavage trials

Small-scale standardization:

$(His)_6$-SUMO-M1 (Section 3.1) was used for small-scale standardization of SUMO tag cleavage. Reaction volumes tried were 250 µL and 120 µL. Each reaction involved protein, 300 mM KCl, 50 mM Tris pH 8, and Ulp1 protease. The amount of protein ($(His)_6$-SUMO-M1) used was 10 µM. Different moles ratio of protease and protein tried were 1:25, 1:50, 1:100 and 1:200 where protease was on the lower side. After the addition of protease, reactions were incubated at 4 ^{O}C for 2 hours, and at different time points, reactions were spun at 15000 rpm for 5 minutes and samples were taken from both pellet and supernatant to check by SDS PAGE for monitoring completion of cleavgae reaction.

Large-scale standardization:

Large-scale standardization of SUMO tag cleavage was done using $(His)_6$-SUMO-M1-Strep (Section 3.3). Large scale refers to SUMO tag cleavage done after processing culture pellets of a volume of 1 L or more. Different conditions were tried, and the details are given in section 3.3.8.

2.4 Thermal shift assay for stability analysis

Thermal shift assay works under the principle of fluorescent dye Sypro Orange, which exhibits higher fluorescence when bound ot hydrophobic patches of a protein (Steinberg et al., 1996). Fluorescence is monitored for the bound dye to unfolded or hydrophobic regions of protein as we subject the protein to a wide range of temperatures. This assay was done to analyse the stability of protein at different buffer conditions, different nucleotide conditions, etc. The total volume of the reaction was 25 µL. The components of the reaction were protein, buffer of interest, $MgCl_2$, nucleotide (if any) & Sypro Orange dye (Sypro orange protein gel stain 5000x Sigma-Aldrich). From the stock of Sypro Orange (5000x), dilution of 50x, and then 5x was made for ease of pipetting. From 5x, it was added into the 25 µL reactions so that final concentration of Sypro Orange was 1x. 25 µL of buffer blank (all the components except the protein) was also kept along with other reactions. The reactions were added to different wells of Biorad 96-well white multi plate PCR plates. After that, these wells are covered with Biorad microseal 'B' seals. The 96-well plate was then given a short spin in a table top centrifuge. After this, the plate was kept inside a Biorad C1000 Touch Thermal Cycler. The protocol was set in such a way that initially, the plate was maintained at 4 ^{O}C for 10 minutes. Then temperature was increased by 0.4 ^{O}C at a rate of 1.6 ^{O}C per second. This was continued till the temperature reached 90 ^{O}C. Relative Fluorescence intensity was measured after each and every increment by 4 ^{O}C. RFU vs Temperature (^{O}C) & -dRFU/dT vs Temperature (^{O}C) was plotted and melting temperature T_m was estimated. Based on the relative T_m values, most stable conditions for the protein were identified.

2.5 Malachite green assay for phosphate estimation

Malachite green assay was done to estimate the ATPase activity of different constructs. The major components required for the assay were filtered malachite green solution (made by dissolving 44 mg of malachite green powder [Sigma-aldrich - Malachite Green Carbinol Base] in 36 ml of 3N H_2SO_4), filtered 7.5 % ammonium molybdate solution

(0.75 g of ammonium molybdate was dissolved in filtered milli-Q and made up to 10 ml) and filtered 11% Tween 20 (11.1 ml of Tween 20 mixed with 8.9 ml milli-Q). 400 µM filtered NaH_2PO_4 was used to make phosphate standards ranging from 25 µM to 200 µM (0, 25, 50, 75, 100, 150 & 200 µM). Three types of reactions were kept: reaction with both protein and ATP, reaction with only protein and the one with only ATP. 1mM $MgCl_2$ was added in all reactions. The ATP concentration used for the reaction was 1 mM. All the reactions were of a total volume of 25 µL (20 µL of reaction + 5 µL of 0.5 M EDTA added to stop the reaction at the end time point). The activity was measured at three time points: 0 minutes, 30 minutes and 60 minutes. In a 96 well plate (Tarsons skirted 96 well 0.2 ml plate), 5 µL of 0.5 M EDTA was already added in different wells and kept. At each time point, 20 µL of reaction was added to wells with EDTA in order to quench the reaction. After quenching all reactions, 50 µL of malachite-ammonium molybdate solution (1 ml solution was made of 800 µL of malachite green solution & 200 µL of 7.5% ammonium molybdate. Also, 16 µL of 11% Tween 20 (to stabilize the complex) was added all the wells. After this, absorbance was measured at 630 nm in CLARIOstar Plus multimode microplate reader (BMG LABTECH). For the standards, concentration vs absorbance (from absorbance values, the absorbance of 0 µM NaH_2PO_4 was subtracted) was plotted. From the slope, the concentration of free phosphate in different reactions was measured. The apparent rate constant, $k_{obs,}$ was calculated by dividing the phosphate concentration by protein concentration and incubation time.

2.6 Pelleting assay for monitoring polymerization

Pelleting assay was done to see whether polymers were formed by the protein as polymers are expected to pellet down when they are spun at high speed (100000 xg). Assay was tried with different protein concentrations as well as different nucleotide conditions. Each reaction was of a volume of 25 µL. The concentration of protein tried was 10 µM and 5 µM and was tried in the absence and presence of 2 mM ATP. 2 mM $MgCl_2$ was added in all the reactions. The reactions were added into ultracentrifuge (Beckman Coulter Optima MAX-XP Ultracentrifuge) tubes. They were placed in TLA

120.2 rotor. Samples were spun for 20 minutes at 100000 xg at 4 ^{O}C. Once the spin was over, the supernatant was transferred to a fresh vial, and the pellet was washed with 200 µL buffer without disturbing the pellet to remove extra of supernatant. After wash pellet was resuspended in the same volume as that of the reaction volume (25 µL). Samples for gel were taken from both supernatant and resuspended pellet to check via SDS PAGE.

2.7 CD Spectroscopy for secondary structure estimation

Circular dichroism (CD) spectroscopy was done to check whether the protein has secondary structures. Spectra were obtained for the far UV region, and the spectropolarimeter used was Jasco J-815. Protein was diluted to 10 µM in 300mM KCl and 50 mM tris pH 8. 10 µM protein was added in a 1 mm cuvette for recording. A digital integration time of 2s, 1 nm bandwidth and a scan speed of 50 nm/min was used. Absorbance was recorded for wavelengths from 200 to 250 nm at room temperature (25 ^{O}C). 15 spectra were averaged in total.

2.8 TEM to check filament formation

Transmission Electron Microscopy (TEM) was used to check whether ScM1 forms filaments. Protein was spun at 22000 xg for 15 minutes. 10 µM and 20 µM dilutions of protein were made after that. Prior to the addition of protein, the carbon formvar grids (TED-PELLA Inc, 300 Mesh) were glow discharged for 25 seconds with a single round of 15 mA current using plasma cleaner (Quorum Technologies). 10 µL of protein (10 µM or 20 µM) was added on to the grid and was incubated for 3 minutes at room temperature. Protein was then blotted out using Whatman paper. After this 10 µL of filtered Milli-Q was added on to the grid, and was blotted immediately. 4 µL of uranyl acetate (0.5 % or 1 %) was added on to the grid and incubated for 15 seconds at room temperature and then blotted out. Before imaging using TEM (JEM - 2200FS Joel Ltd.), the grids were dried.

Chapter - 3
Results

3.1 Characterization of $(His)_6$-SUMO-MreB1

The construct was designed such that ScM1 has a SUMO tag at its N-terminus to improve solubility and expression. All the details, starting from cloning to characterization are given in the following sections.

3.1.1 Cloning of $(His)_6$-SUMO-M1:

pHis17_M1 was used as template for PCR 1. Primers used for PCR 1 are shown in table 2.1 (sequences in red correspond to gene, and those in blue correspond to that of pET28a vector). ~ 1.1 Kb amplification was visible on agarose gel after PCR 1 (Fig. 3.1 A). pET28a_FtsA (FtsA gene at the C terminus of SUMO tag) was the template for PCR 2. Details of PCR 1 and PCR 2 are given in tables 2.2, 2.3 and 2.4. After PCR 2, DpnI digestion was done, followed by electroporation transformation. Test plate had lot of colonies, and control plate was clean. Five colonies were screened, and a clone check PCR (Fig. 3.1 B) was done using gene specific primers. pHis17_M1 was kept as positive control. All clones, including positive control, had an amplification corresponding to the expected size of 1042 bp. Two out of five clones were positive (positive - release length of ~1 Kb, negative - release length of ~ 1.3 Kb) from double digestion check (NdeI and BamHI). Both were sent for sequencing. Plasmid 2 came to be positive. It was transformed into expression strains for expression check.

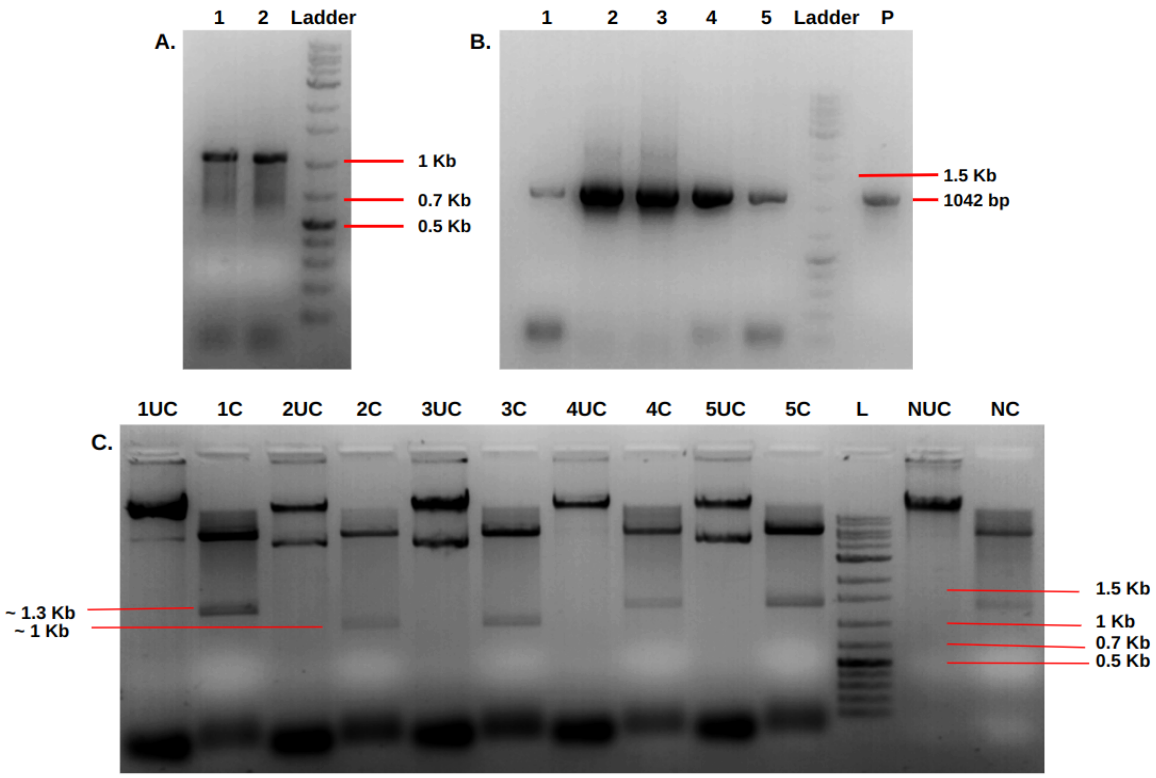

Fig. 3.1: **Agarose gel image of cloning of $(His)_6$-SUMO-M1**. A) Agarose gel image after PCR 1. Two 50 µL reactions were subjected to PCR (lanes 1 and 2). B) Agarose gel image after PCR for confirming positive clones. 1 to 5 are five probable clones, while P refers to positive control C) Agarose gel after double digestion. ”UC” refers to uncut, “C” refers to cut and “N” refers to the negative control.

3.1.2 Expression check of $(His)_6$-SUMO-M1:

pET28a_$(His)_6$-SUMO-M1 (kanamycin resistant) was transformed into BL21AI and Rosetta-DE3 to check expression and solubility. Fig. 3.2 shows the gel image for expression check. Both the strains showed good expression and almost 100% solubility, but comparatively, the protein was slightly better expressed in Rosetta-DE3 cells. So pET28a_$(His)_6$-SUMO-M1 was transformed into Rosetta to grow large cultures before protein purification.

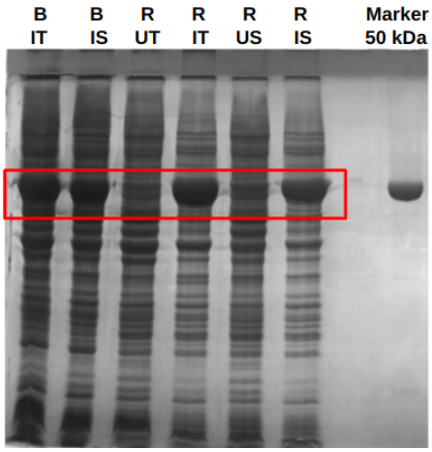

Fig. 3.2: **Expression check of $(His)_6$-SUMO-M1.** SDS-PAGE gel image after expression check. "B" - BL21AI, "R" - Rosetta, "U" - uninduced, "I" - induced, "T" - total, "S" - supernatant . The expected band size is highlighted within the red box.

3.1.3 Purification of $(His)_6$-SUMO-M1

For standardizing purification of $(His)_6$-SUMO-M1 to achieve maximum purity and yield, different methods were tried as given below.

Trial 1: Ni-NTA affinity chromatography followed by gel filtration:

1 L culture (Rosetta-DE3) pellet of $(His)_6$-SUMO-M1 was processed. 50 mM imidazole concentration was maintained in lysis buffer and binding buffer (Buffer A, Table 2.14) to avoid possible non-specific binding of other proteins during Ni-NTA affinity chromatography (Fig. 3.3 A). After Ni-NTA, the best fractions were pooled together and were concentrated to 1 ml. Concentrated protein was loaded onto the size exclusion column (BioRad 650). The peak in the elution profile was spread from void to monomer and, most of the protein came in void (Fig. 3.3 C). The total yield of $(His)_6$-SUMO-M1 obtained was 28 mg/ml (~800 µL in volume).

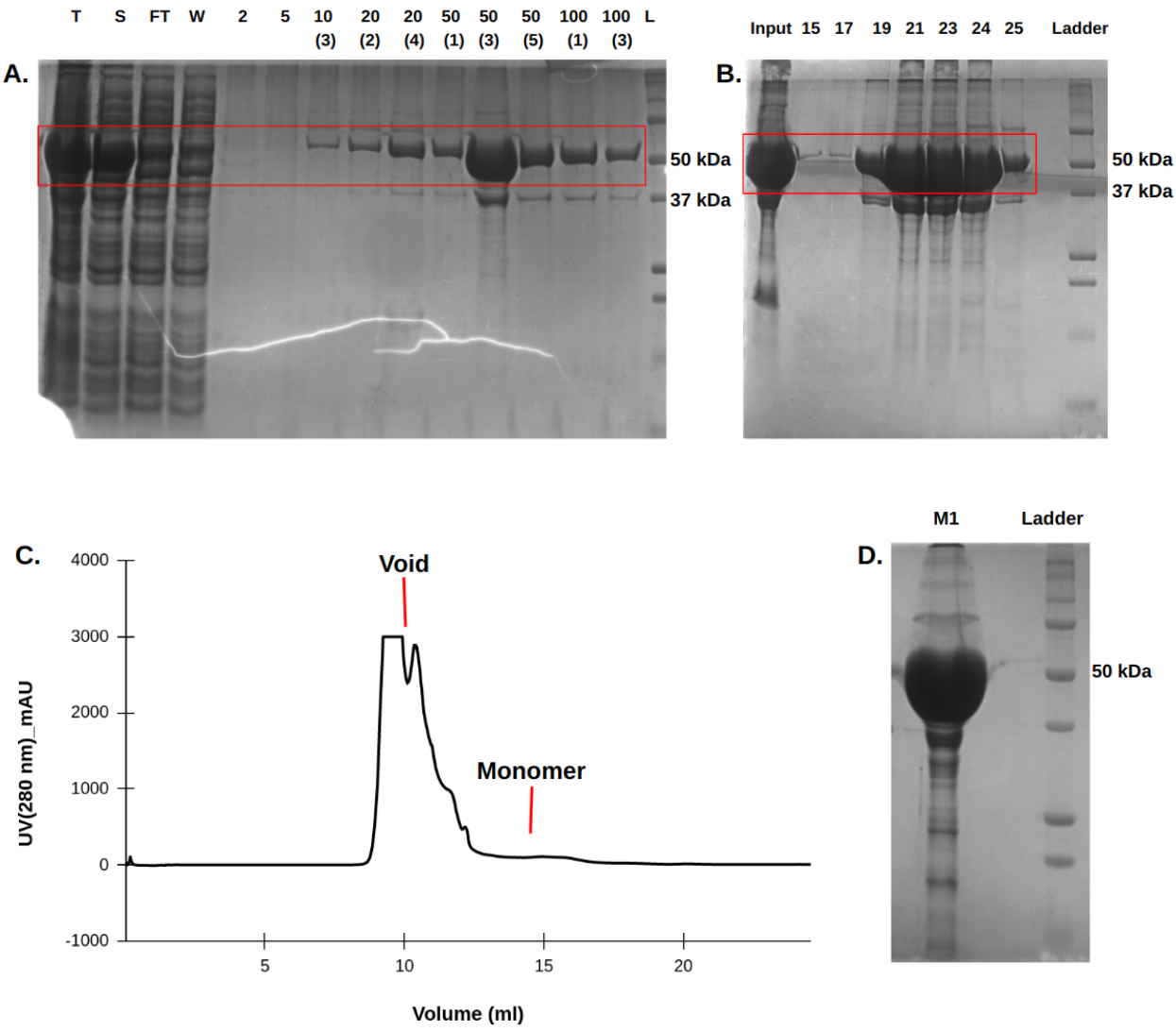

Fig. 3.3: **Two step purification of $(His)_6$-SUMO-M1** A) SDS-PAGE gel image after Ni-NTA affinity chromatography B) SDS-PAGE gel image after size exclusion chromatography. C) BioRad 650 elution profile of $(His)_6$-SUMO-M1 D) Purity check gel image. The expected band size is highlighted within the red box. "T" - Total cell lysate fraction, "S" - Supernatant, "FT" - Flow through, "W" - Wash & "L" - ladder.

Trial 2: Purification exclusively from Ni-NTA:

1 L culture (Rosetta-DE3) pellet of $(His)_6$-SUMO-M1 was processed. 50 mM imidazole concentration was maintained in lysis buffer and binding buffer (Buffer A, Table 2.14) to avoid possible non-specific binding of other proteins during Ni-NTA affinity chromatography (Fig. 3.4 A). After Ni-NTA, best fractions were pooled together and were subjected to dialysis (Table 2.14). After 2 hours of dialysis, protein was

concentrated. The final yield of $(His)_6$-SUMO-M1 obtained was 18 mg/ml (~ 1 ml in volume).

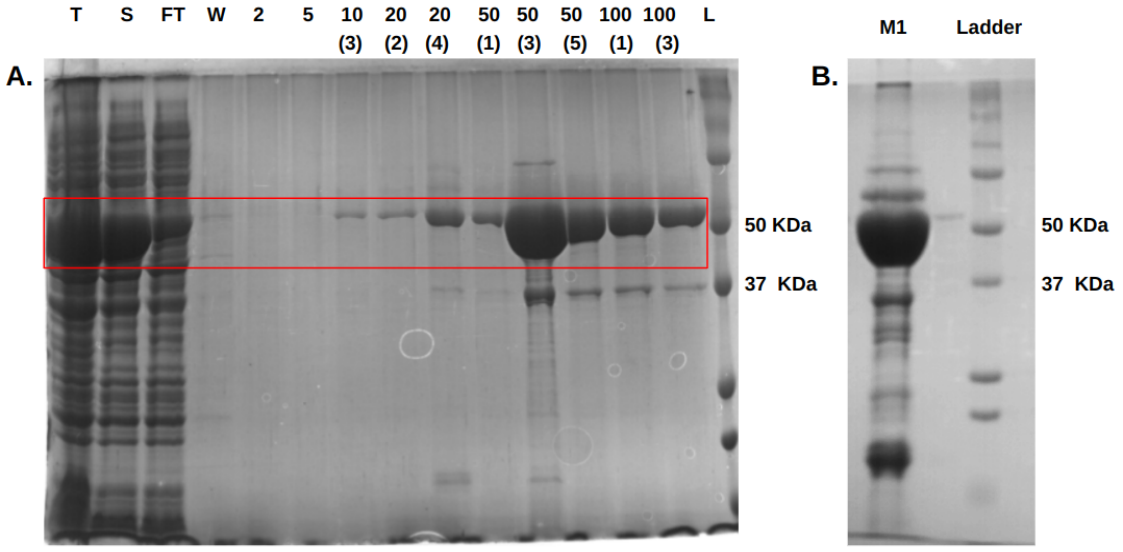

Fig. 3.4: **Ni-NTA purification of $(His)_6$-SUMO-M1** A) SDS-PAGE gel image after Ni-NTA affinity chromatography B) SDS-PAGEgel image after purity check. The expected band size is highlighted within the red box. "T" - Total cell lysate fraction, "S" - Supernatant, "FT" - Flow through, "W" - Wash & "L" - ladder.

Trial 3: Purification of Untagged ScM1:

2 L culture (Rosetta-DE3) pellet of $(His)_6$-SUMO-M1 was processed. 50 mM imidazole concentration was maintained in lysis buffer and binding buffer (Buffer A, Table 2.14) to avoid possible non-specific binding of other proteins during Ni-NTA affinity chromatography (Fig. 3.5 A). After Ni-NTA, best fractions were pooled together and were subjected to dialysis to remove imidazole. SUMO protease (Ulp1) was added to protein during dialysis (1:100 moles ratio of SUMO protease:protein) for removal of SUMO tag. A lot of protein started precipitating during dialysis post cleavage. After two hours of dialysis, protein was spun at 15000 rpm, for 15 minutes (4 ^{O}C). After this, second Ni-NTA (Fig. 3.5 B) was done to get untagged protein. Protein came in flow through and wash as expected. The cleaved SUMO tag was expected to bind to the column and to get eluted at higher concentration of buffer B (Table 2.14) but SUMO tag eluted in flow through and wash also. The fractions with untagged M1 was concentrated

to 1 ml (concentration was 1.5 mg/ml) and then gel filtration (Biorad 650) was done to get SUMO tag separated from M1. The tag got very well separated (Fig. 3.5 D) but the amount of M1 that was eluted after size exclusion chromatography was very less. Therefore fractions were not concentrated. As most of the protein was lost after the removal of the SUMO tag, Ulp1-based cleavage had to be standardized with respect to the amount of protease and incubation time (Section 3.1.9).

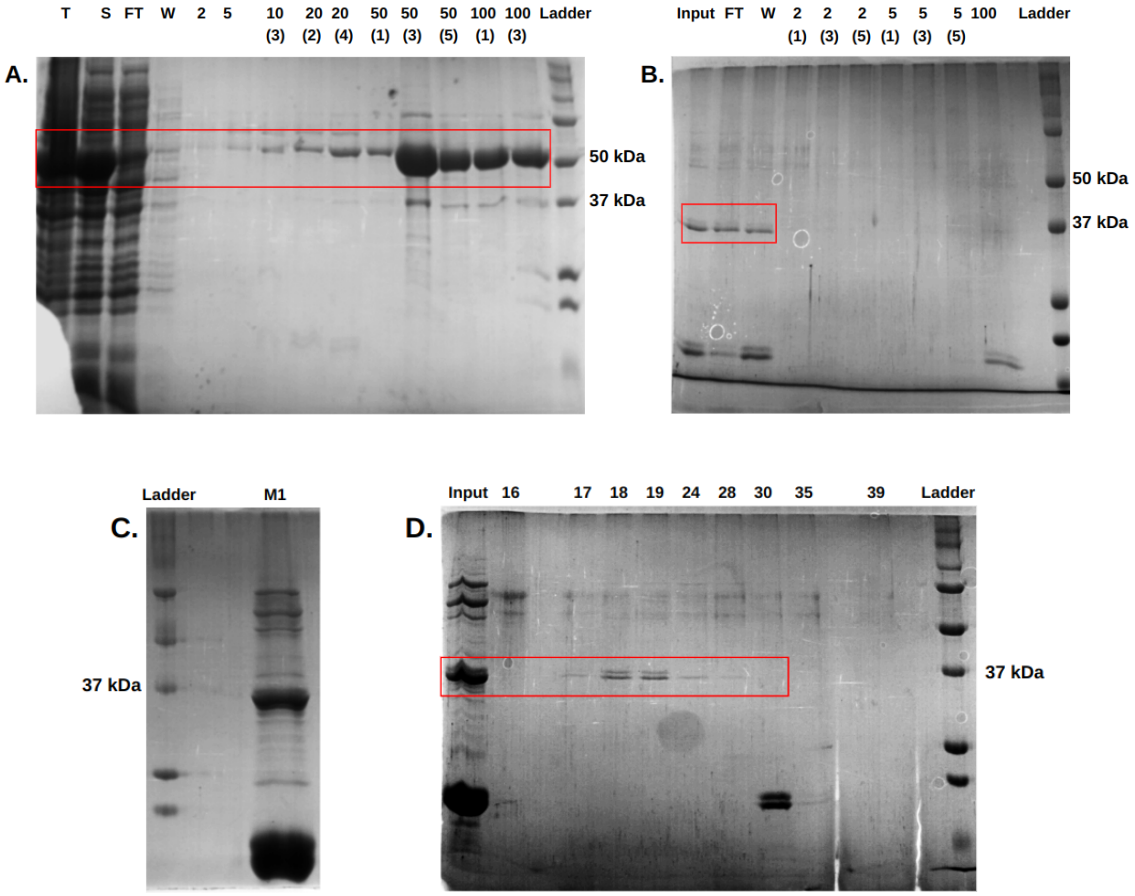

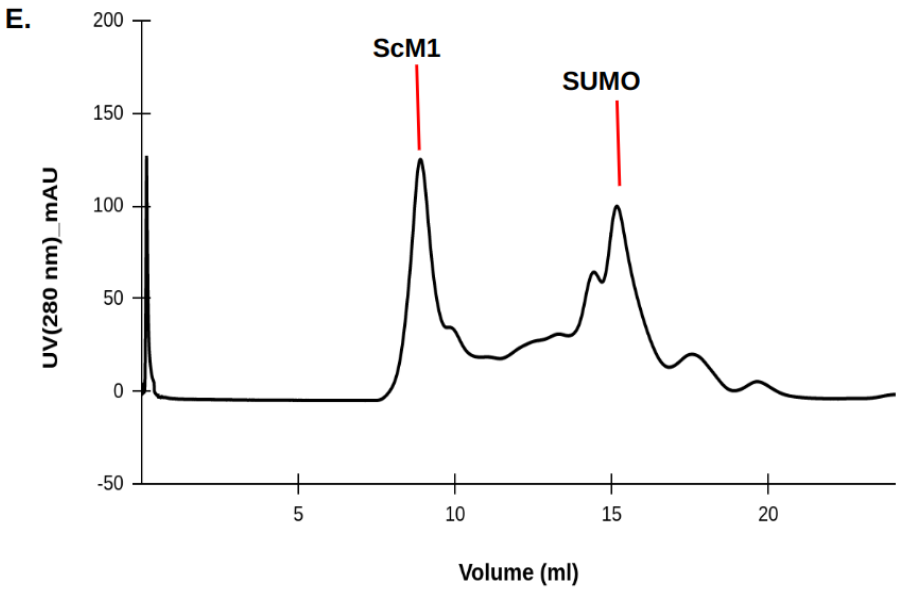

Fig. 3.5 : **Attempt to purify untagged ScM1** A) SDS-PAGE gel image after Ni-NTA affinity chromatography B) SDS-PAGE gel image after second Ni-NTA chromatogrphy post SUMO tag cleavage. C) SDS-PAGE gel image showing purity of concentrated untagged M1 post second Ni-NTA chromatogrphy. D) SDS-PAGE gel image after size exclusion chromatography. E) Biorad 650 elution profile of untagged M1. The expected band size is highlighted within the red box. “T” - Total cell lysate fraction, “S” - Supernatant, “FT” - Flow through & “W” - Wash

3.1.4 SUMO tag cleavage standardization

The 250 µL reaction having protease and protein (10 µM) was incubated for 2 hours. 1:50 and 1:100 moles ratio (protease:protein) were tried. Samples were taken from both supernatant and pellet fractions at different time points and checked on SDS PAGE gel (Fig. 3.6 A & Fig. 3.6 B). In Fig. 3.6 A & Fig. 3.6 B, more protein seems to be in pellet fraction as mistakenly the resuspension of pellets was not done in the same volume as that of the reaction, but from these two gels, it was clear that cleavage was done within 30 to 60 minutes itself and there was no need to wait for 2 hours. In the second round of standardization, a 120 µL reaction having protease and protein (10 µM) was incubated for 30 minutes.1:25, 1:50, 1:100 and 1:200 moles ratio (protease:protein) were tried. Samples were taken from both supernatant and pellet fractions at 15 and 30 minutes time points and checked on SDS PAGE gel (Fig. 3.6 C & Fig. 3.6 D). More amount of protein was seen to precipitate when the amount of protease added was

higher than the ratio of 1:100. So it was concluded that a 1:200 or 1:100 moles ratio with an incubation time of 30 to 40 minutes would be sufficient for complete and efficient cleavage of SUMO tag.

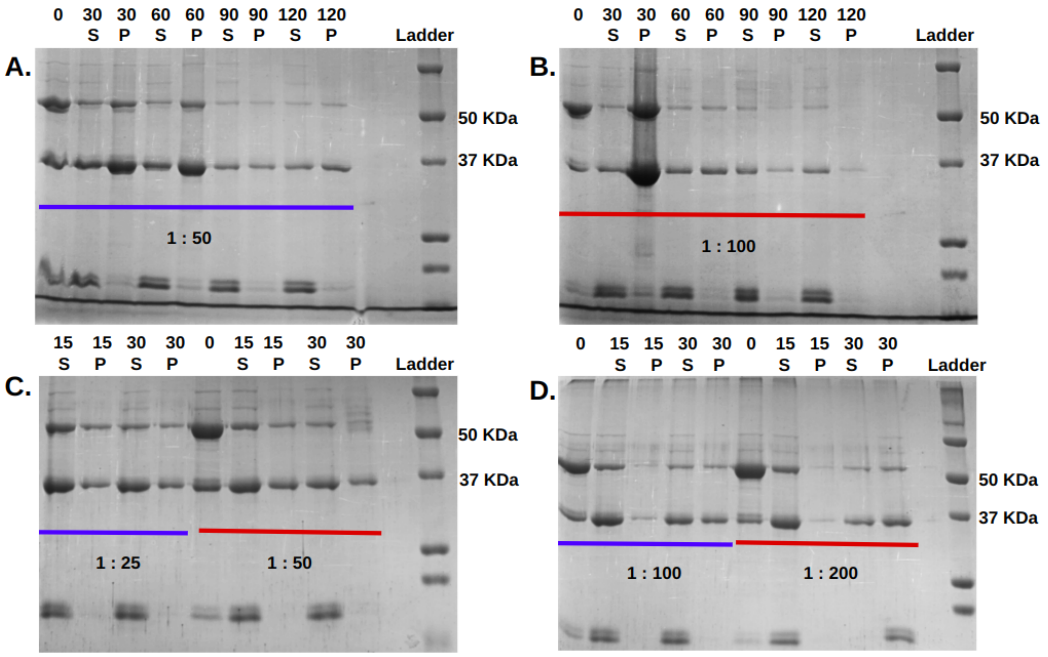

Fig. 3.6: **SDS-PAGE gel images depicting standardization of Ulp1 mediated SUMO tag cleavage** A) 1:50 moles ratio (250 µL reaction; 0, 30, 60, 90, 120 minutes time point). B) 1:100 moles ratio (250 µL reaction; 0, 30, 60, 90, 120 minutes time point). C) 1:25 & 1:50 moles ratio (120 µL reaction; 0, 15, 30 minutes time point). D)1:100 & 1:200 moles ratio (120 µL reaction; 0, 15, 30 minutes time point)

3.1.5 Thermal shift assay for stability analysis

This assay was tried for $(His)_6$-SUMO-M1 under different buffer and nucleotide conditions. The difference in stability was analysed for KCl and NaCl buffers (in Tris pH 8). At the same time, both the buffer conditions were tried with and without the presence of ADP. As observed in the graph, the dye was showing high fluorescence at the very start itself. The data obtained was incolclusive as the T_m could not be estimated.

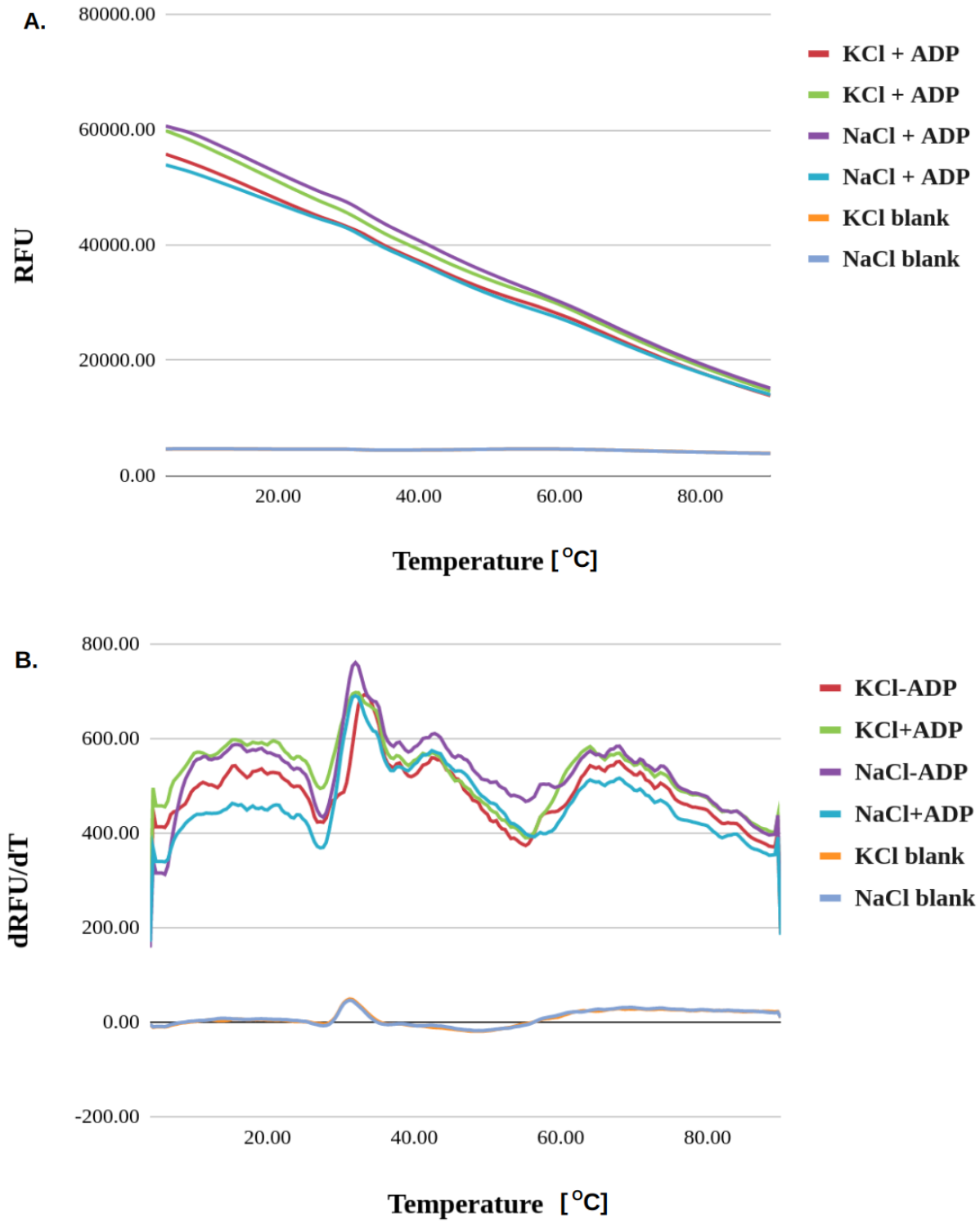

***Fig. 3.7*: Stability analysis plots of $(His)_6$-SUMO-M1** A) RFU vs Temperature plot for $(His)_6$-SUMO-M1 B) First derivative of RFU vs Temperature plot for $(His)_6$-SUMO-M1

3.1.6 Malachite assay to quantify ATPase activity

Malachite assay was tried for two different concentrations (5 μM and 10 μM) of $(His)_6$-SUMO-M1. M5-$(His)_6$ (*Spiroplasma citri* MreB5 with a hexahistidine tag at the C-terminus) was used as a positive control for which the activity was already characterized in our lab. The mean k_{obs} obtained for different concentrations of protein and positive control are given in table 3.1. Scatter plot comparing wild type and mutant is shown in fig. 3.14.

Table 3.1 : ATPase activity of $(His)_6$-SUMO-M1

Protein	Concentration (μM)	No. of repeats	k_{obs} (min^{-1})
$(His)_6$-SUMO-M1	5	6	0.105 ± 0.003
$(His)_6$-SUMO-M1	10	8	0.132 ± 0.008
M5-$(His)_6$	10	4	0.118 ± 0.009

3.1.7 Pelleting assay

The assay was tried with 5 μM and 10 μM of $(His)_6$-SUMO-M1. After spinning at a speed of 100,000 xg also, most of the protein was in supernatant. There was no difference in the presence or absence of 2 mM ATP.

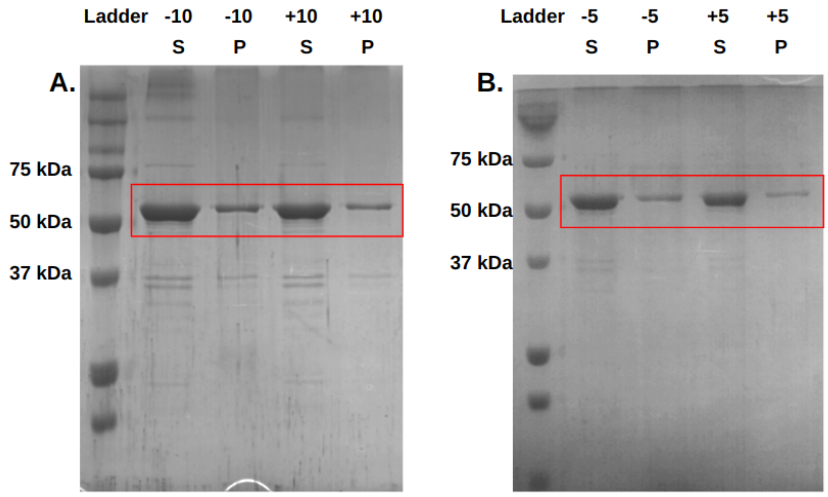

***Fig 3.8*: Pelleting assay for $(His)_6$-SUMO-M1.** A) SDS-PAGE gel image of pelleting assay with and without ATP for 10 µM of $(His)_6$-SUMO-M1. B) SDS-PAGE gel image of pelleting assay with and without ATP for 5 µM of $(His)_6$-SUMO-M1. The expected band size is highlighted within the red box. "+" – ATP addition, "-" – No ATP addition, "10" – Protein concentration of 10 µM, "5" – Protein concentration of 5 µM "P" – Pellet fraction, "S" – supernatant fraction.

3.1.8 CD spectroscopy for secondary structure estimation

10 µM of $(His)_6$-SUMO-M1 was used for CD spectroscopy. Buffer A (Table 2.14) was used as buffer control. The plot obtained after CD (Fig. 3.9) spectroscopy showed that the protein has intact secondary structures.

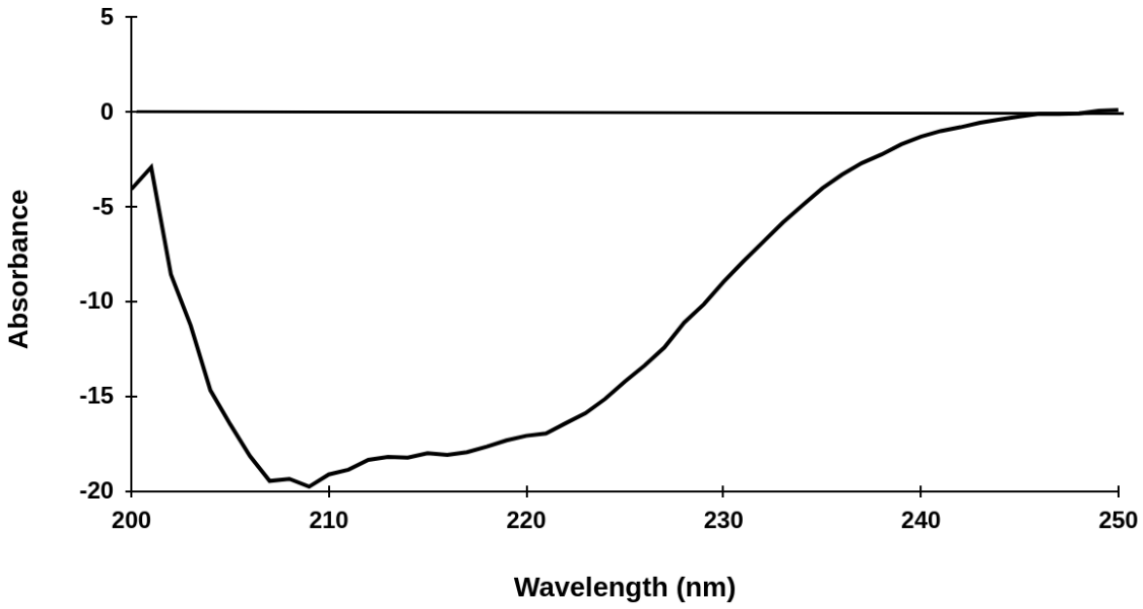

***Fig. 3.9*: Secondary structure estimation of $(His)_6$-SUMO-M1 .** Absorbance vs wavelength plot after CD spectroscopy of $(His)_6$-SUMO-M1.

3.2 Characterization of $(His)_6$-SUMO-M1 - E137A

To confirm that the ATPase activity was shown by $(His)_6$-SUMO-M1 itself and not from any other impurities, an ATPase mutant was designed. Another reason for this was due to the difference in ATPase activity of ScM1 in two different constructs (ScM1-$(His)_6$ - 0.49 min^{-1} [previously estimated in the lab] and $(His)_6$-SUMO-M1 - 0.114 ± 0.018 min^{-1}). In the already characerized *Caulobacter crescentus* (CcMreB), it was observed that E140 is necessary for the positioning of catalytic water appropriately in proximity of the γ-phosphate for its hydrolysis (van den Ent et al., 2014). For CcMreB and ScM5, mutating this residue (E134 in the case of ScM5) led to the inhibition of ATPase activity (van den Ent et al., 2014)(Pande et al., 2022). This glutamate is very well conserved across other ScMreBs as well. So, the residue (E137) corresponding to CcMreB E140 was mutated to alanine in ScM1. For ScM1-$(His)_6$, E137A was ATPase inactive [previously done in the lab].

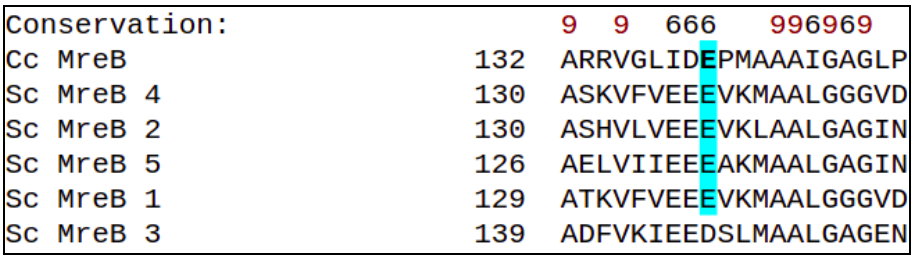

Fig. 3.10: **Sequence alignment of five ScMreBs with CcMreB.** The conservation of catalytically active glutamate in highlighted in cyan.

3.2.1 Cloning of $(His)_6$-SUMO-M1 - E137A:

pET28a_$(His)_6$-SUMO-M1 was used as template for PCR 1. Primers used for PCR 1 are shown in table 2.1 (Sequences in red correspond to gene, blue correspond to that of pET28a vector, and those highlighted in yellow corresponds to the mutation). Around 0.67 Kb amplification was visible on agarose gel after PCR 1 (Fig. 3.11). pET28a_$(His)_6$-SUMO-M1) itself was used as template for PCR 2. Details of PCR 1 and PCR 2 are given in tables 2.5 and 2.6. Temperature conditions for PCR were kept similar to that of wild type (Table 2.4). After PCR 2, DpnI digestion was done, followed by electroporation transformation. Test plate had lot of colonies, and control plate was clean. As the template and insert used for PCR 2 had M1 gene, clone check PCR using gene specific primers were of no relevance. Double digestion check was also of no use for the same reason. Three samples were sent for sequencing. One of the clones came positive.

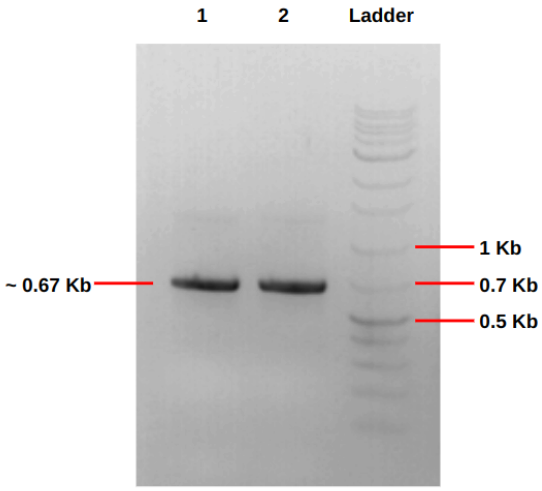

Fig 3.11: **Agarose gel image after PCR 1.** Lanes 1 and 2 denote two parallel reactions of PCR 1 with 0.67 kb amplified product

3.2.2 Expression check of $(His)_6$-SUMO-M1 - E137A:

pET28a_$(His)_6$-SUMO-M1 - E137A (Kanamycin resistant) was transformed into Rosetta-DE3 for expression check. It showed very good expression (Fig. 3.12) and solubility similar to that of the wild type. This was therefore transformed into rosetta to grow large cultures before protein purification.

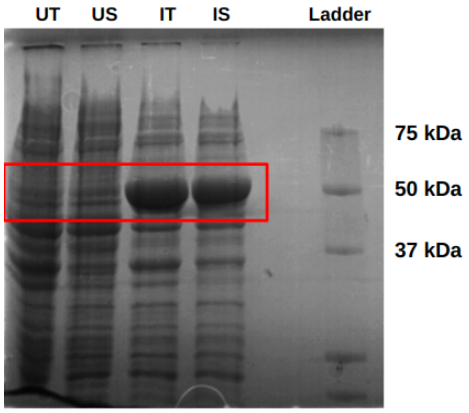

Fig. 3.12: **Expression check of $(His)_6$-SUMO-M1 - E137A.** SDS-PAGE gel image after expression check. The expected band size is highlighted within the red box. “U” - uninduced, “I” - induced, “T” - total, “S” - supernatant

3.2.3 Purification of $(His)_6$-SUMO-M1 - E137A

2 L culture (Rosetta-DE3) pellet of $(His)_6$-SUMO-M1 - E137A was processed. When 50 mM imidazole concentration was maintained in lysis buffer and binding buffer (Buffer A, Table 2.14) similar to purification of wild type, protein was eluted in wash and 2% fractions. After multiple trials, it was finalized that 10 mM imidazole was the maximum possible amount which could be maintained in buffer A and lysis buffer to avoid binding of unknown proteins. After Ni-NTA, best fractions were pooled together and were subjected to dialysis (table 2.14). After 2 hours of dialysis, protein was concentrated. The final yield of $(His)_6$-SUMO-M1 - E137A obtained was 10 mg/ml (~ 1.2 ml in volume). 500 µL (3 mg/ml) of protein was injected into gel filtration system (BioRad 650) for an analytical run (Fig. 3.13 C). The peak obtained was similar to wild type, that is, the peak was spread from void to monomer.

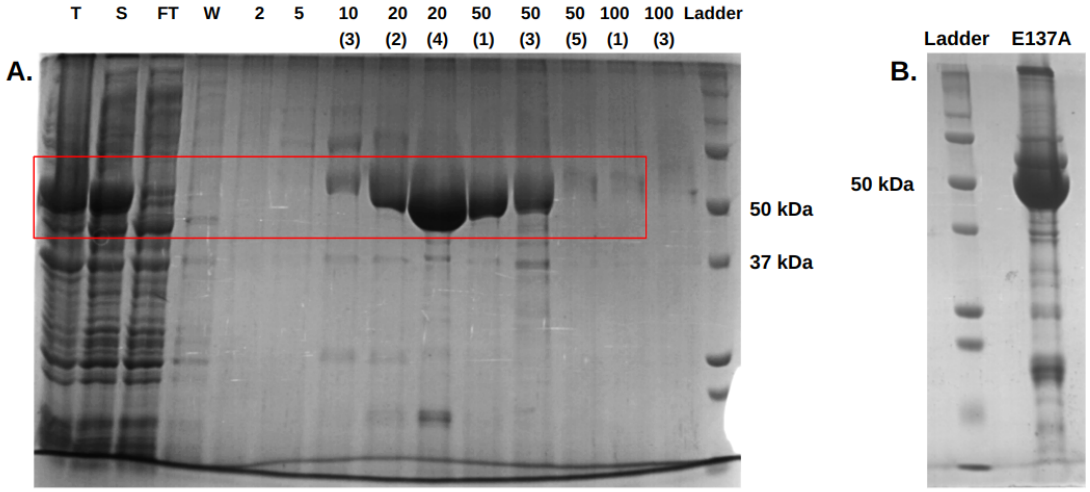

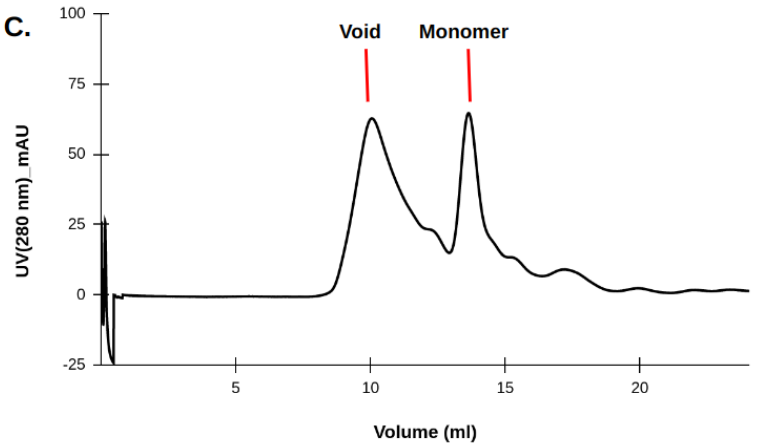

Fig. 3.13: **Ni-NTA purification of $(His)_6$-SUMO-M1 - E137A.** A) SDS-PAGE gel image after Ni-NTA affinity chromatography B) SDS-PAGE gel image after purity check C) Biorad 650 elution profile of $(His)_6$-SUMO-M1 - E137A obtained after an analytical run in biorad 650. The expected band size is highlighted within the red box. "T" - Total cell lysate fraction, "S" - Supernatant, "FT" - Flow through & "W" - Wash

3.2.4 Malachite assay to quantify ATPase activity

Malachite assay was tried for 10 µM of $(His)_6$-SUMO-M1 - E137A. $(His)_6$-SUMO-M1 (Wild type) was used as a positive control for the assay. The mean k_{obs} obtained for the mutant and positive control are given in table 3.2. Surprisingly, the mutant showed higher activity than the wild type $(His)_6$-SUMO-M1. Scatter plot which compares activity of wild type and mutant is given below (Fig. 3.14)

Table 3.2: ATPase activity of $(His)_6$-SUMO-M1-E137A

Protein	Concentration (µM)	No. of repeats	k_{obs} (min^{-1})
$(His)_6$-SUMO-M1	10	8	0.132 ± 0.008
$(His)_6$-SUMO-M1-E137A	10	3	0.220 ± 0.005
M5-$(His)_6$	10	4	0.118 ± 0.009

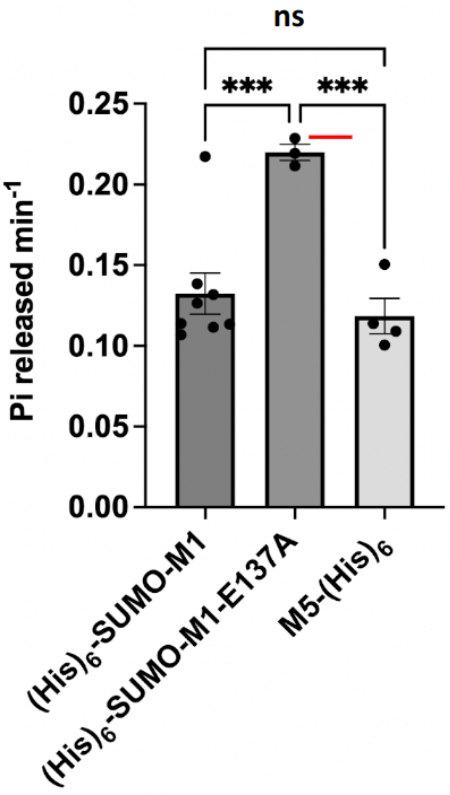

Fig. 3.14 : **Plot for comparison of ATPase activity of $(His)_6$-SUMO-M1 and $(His)_6$-SUMO-M1 - E137A.** Y-axis shows k_{obs} of $(His)_6$-SUMO-M1, $(His)_6$-SUMO-M1 - E137A and M5-$(His)_6$. The data point marked by the red line denotes k_{obs} obtained from a different purified batch of the same construct. 2 way Annova test was used to compare the activity between constructs. “ns” refers to “not significant” (p-value = 0.93). (***) - denotes significant difference. *** on left side corresponds to a p-value of 0.0008 and *** on the right side corresponds to a p-value of 0.0010.

3.3 Characterization of $(His)_6$-SUMO-M1-Strep

The major aim behind designing $(His)_6$-SUMO-M1-Strep was to improve the purity. As strep affinity chromatography is very specific, it was thought to improve the purity compared to that of while passing it through Ni-NTA column. This would also help in separating the SUMO tag from ScM1, following Ulp1 protease cleavage.

3.3.1 Cloning of $(His)_6$-SUMO-M1-Strep:

In this cloning, amplification was done in two steps. pET28a_$(His)_6$-SUMO-M1 was used as the template for PCR 1. Forward primer and reverse primer 1 (refer to table 2.1) were used as primers for the first step (sequences in red correspond to the gene, blue correspond to that of pET28a vector, and those in green correspond to the strep tag). Around 1.1 Kb amplification was visible on agarose gel after the first amplification (Fig. 3.15 A). This amplified product was used as template for the second extension step (to amplify the full-length strep sequence). The primers used were forward primer and reverse primer 2 (Table 2.1). pET28a_$(His)_6$-SUMO-FtsA was used as template for PCR 2. Details of PCR 1 and PCR 2 are given in tables 2.7, 2.8, 2.9 and 2.10. After PCR 2, DpnI digestion was done, followed by electroporation transformation. Test plate had colonies, and control plate was clean. Clone check PCR (using gene specific forward and reverse primers) and double digestion check (NdeI and BamHI) was done for two samples. For PCR check and digestion check, pET28a_$(His)_6$-SUMO-M1 was used as positive control and pET28a_$(His)_6$-SUMO-FtsA was used as negative control. PCR check showed amplification of around 1.1 Kb, and double digestion check had a release length of around 1.1 Kb for both the samples. The clones were sent for sequencing.

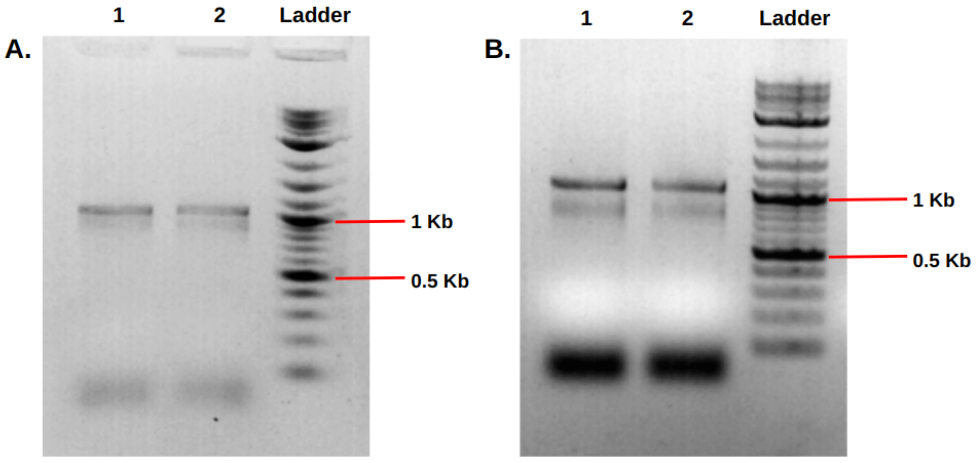

Fig. 3.15: **Two step PCR 1** A) Agarose gel image after Step-1 & B) Step-2 (Extension)

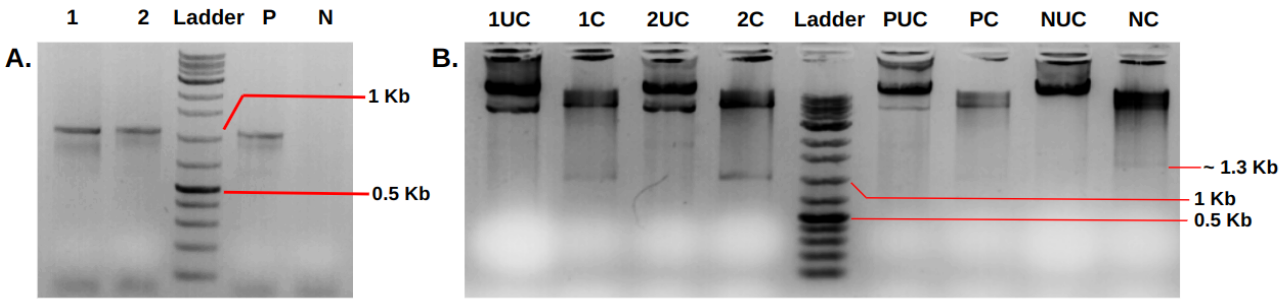

Fig. 3.16: **Agarose gels images of clone check of $(His)_6$-SUMO-M1-Strep** A) Agarose gel image after clone check PCR. 1 and 2 are the clones. B) Agarose gel image after double digestion check. P refers to the positive control, while N denotes the negative control. "C" - Plasmid which was cut, "UC" - Uncut plasmid

3.3.2 Expression check of $(His)_6$-SUMO-M1-Strep

pET28a_$(His)_6$-SUMO-M1-Strep (kanamycin resistant) was transformed into BL21AI and Rosetta-DE3 for expression check. It showed very good expression (Fig. 3.17) and almost 100% solubility in both strains but comparatively, expression was more in the case of Rosetta. This was therefore transformed into Rosetta to grow large cultures before protein purification.

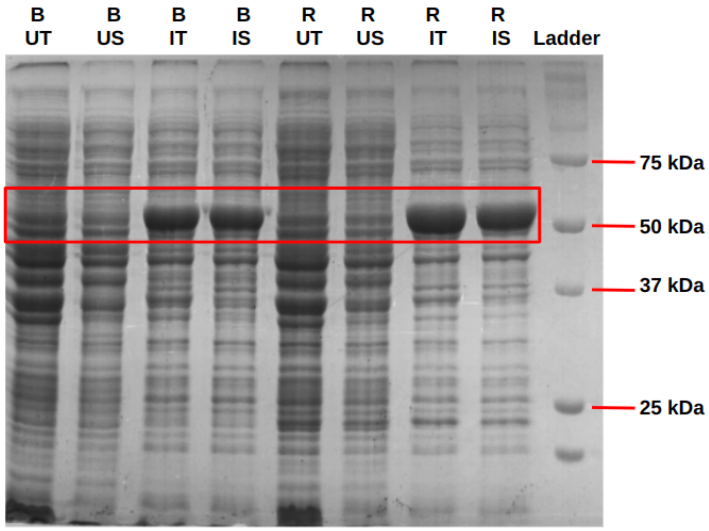

Fig. 3.17: **Expression check of $(His)_6$-SUMO-M1-Strep.** SDS-PAGE gel image after expression check. The expected band size is highlighted within the red box. "B" - BL21AI, "R" - Rosetta, "U" - uninduced, "I" - induced, "T" - total, "S" - supernatant

3.3.3 Purification of $(His)_6$-SUMO-M1-Strep

2 L culture (Rosetta-DE3) pellet of $(His)_6$-SUMO-M1-Strep was processed. 50 mM imidazole concentration was maintained in lysis buffer and binding buffer (Buffer A, Table 2.14) to avoid possible non-specific binding of other proteins during Ni-NTA affinity chromatography (Fig. 3.18 A). After Ni-NTA, best fractions were pooled together and were subjected to dialysis (table 2.14). After 2 hours of dialysis, protein was loaded onto the StrepTrap column. The eluted fractions were then concentrated. The final yield of protein obtained was 1.2 mg/ml (900 µL).

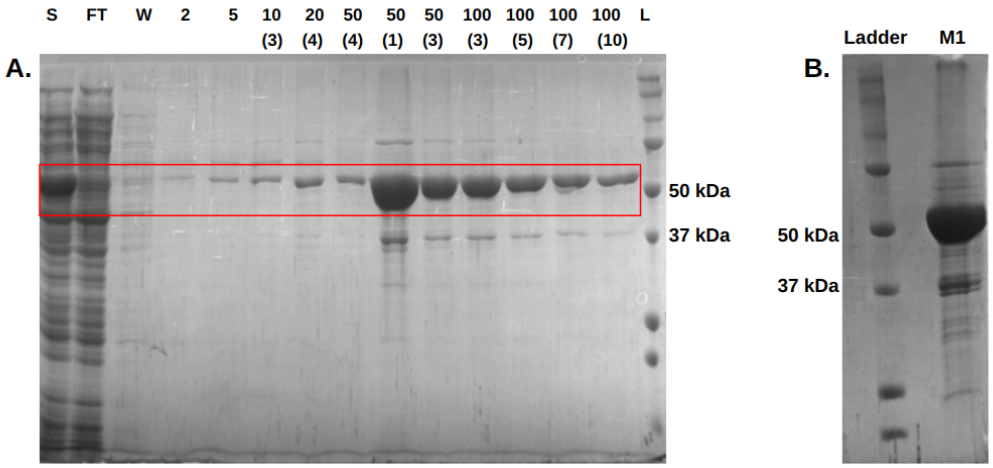

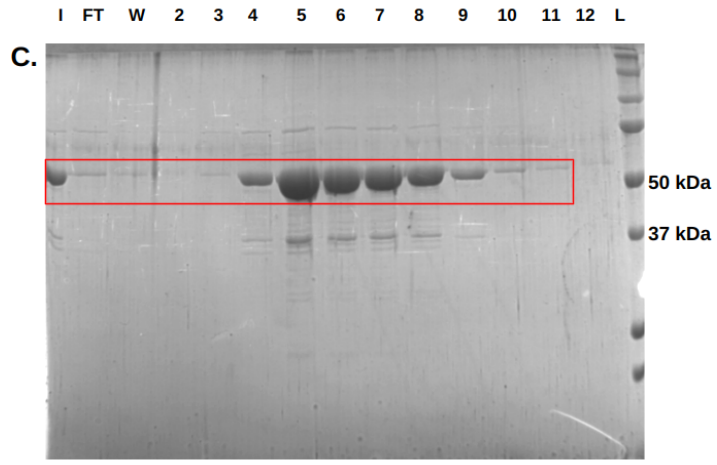

Fig. 3.18: **Two step purification of $(His)_6$-SUMO-M1-Strep** A) SDS-PAGE gel image after Ni-NTA affinity chromatography B) SDS-PAGE gel image of purity check after strep-tag affinity chromatography. C) SDS-PAGE gel image after Strep-tag affinity chromatography. The expected band size is highlighted within the red box "S" - Supernatant, "FT" - Flow through, "W" - Wash, "I" - Input (Sample loaded onto strep column), "L" - ladder.

3.3.4 Malachite assay to quantify ATPase activity

Malachite assay was tried for 10 µM of $(His)_6$-SUMO-M1-Strep. The mean k_{obs} obtained is given in table 3.3. Scatter plot comparing wild type and mutant is shown in fig. 3.29. $(His)_6$-SUMO-M1-Strep was observed to be more active than $(His)_6$-SUMO-M1.

3.3.5 Pelleting assay

Assay was done for 10 µM of $(His)_6$-SUMO-M1-Strep. The amount of protein obtained in pellet was negligible. Also, there was no difference in the amount of protein obtained in pellet in the presence and absence of ATP (Fig. 3.19).

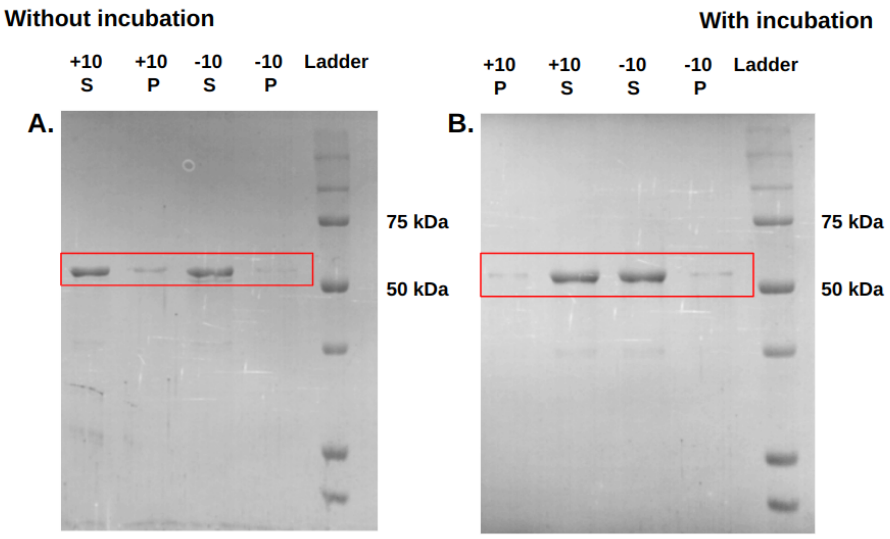

Fig. 3.19: **Pelleting assay for $(His)_6$-SUMO-M1-Strep.** A) SDS-PAGE gel image of pelleting assay with and without ATP for 10 µM of $(His)_6$-SUMO-M1-Strep B) SDS-PAGE gel image of pelleting assay with and without ATP for 10 µM of $(His)_6$-SUMO-M1-Strep with an incubation of 20 minutes at 25 ^{O}C before the ultra centrifuge spin. The expected band size is highlighted within the red box. "+" – ATP addition, "-" – No ATP addition, "10" – Protein concentration (10 µM), "P" – Pellet fraction, "S" – supernatant fraction

3.3.6 CD spectroscopy

10 µM of $(His)_6$-SUMO-M1-Strep was used for CD spectroscopy. Buffer A (Table 2.14) was used as buffer control. From the plot, it was clear that the protein had intact secondary structures.

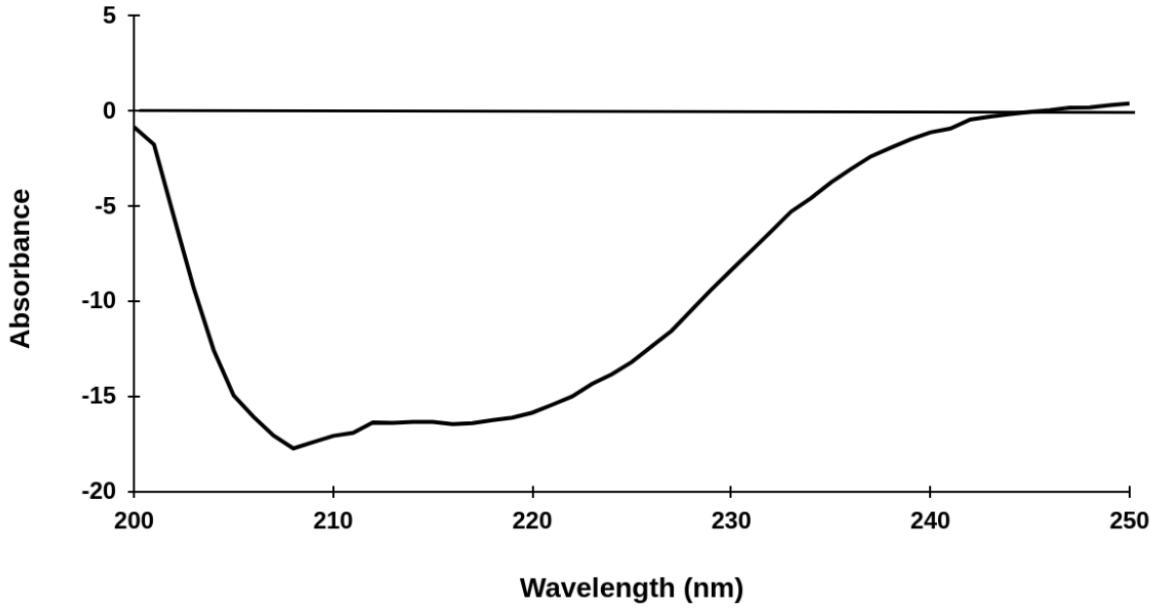

Fig. 3.20: **Secondary structure estimation of $(His)_6$-SUMO-M1-Strep.** Absorbance vs Wavelength plot after CD spectroscopy of $(His)_6$-SUMO-M1-Strep.

3.3.7 Attempts to purify M1-Strep post SUMO tag cleavage

As SUMO tag was almost one-third of the size of the protein, it could have affected the protein in many aspects. It could have led to some artefacts (e.g. it can lead to misinterpretations in interaction studies). In order to get M1-Strep from $(His)_6$-SUMO-M1-Strep, Ulp1 protease-mediated cleavage of the SUMO tag was necessary. Different trials with variations in reaction conditions were attempted to achieve this. Details of different trials are given below.

Trial 1:

2L pellet of $(His)_6$-SUMO-M1-Strep was processed. After Ni-NTA affinity chromatography, dialysis was done to remove imidazole. The eluted volume (52 ml) was then divided into five fractions in 15 ml falcons. Protein concentration (0.4 mg/ml) was estimated using the Bradford assay. Ulp1 protease was then added to falcons in the moles ratio of 1:100 and falcons were incubated in ice for 1 hour. From previous SUMO

tag cleavage standardization (Section 3.1.9), it was found that incubating for more than an hour was not necessary as longer incubation resulted in more lose of protein due to precipitation. After incubation, it was spun and loaded onto the strep column. From the gel, it was clear that the cleavage was not 100 %, and the amount of protein obtained after strep affinity chromatography was also very less.

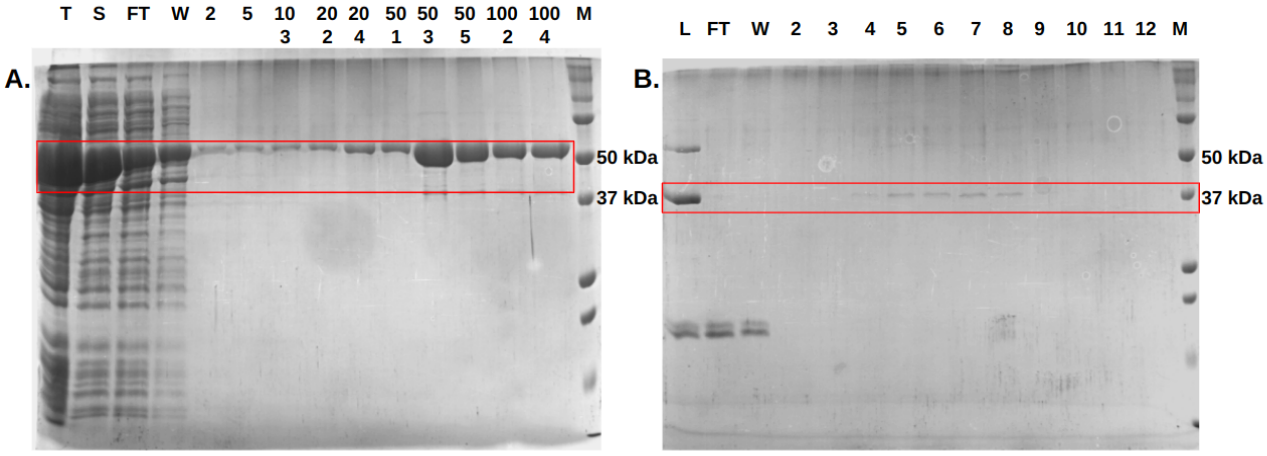

Fig. 3.21: **Trial 1 of large scale SUMO tag cleavage Standardization** A) SDS-PAGE gel image after Ni-NTA purification of $(His)_6$-SUMO-M1-Strep B) SDS-PAGE gel image after Strep affinity purification post SUMO tag cleavage. The expected band size is highlighted within the red box. “T” - Total, “S” - Supernatant, “FT” - Flow through, “W” - Wash, “L” - load (Input for Strep affinity chromatography) & “M” - Ladder

Trial 2:

As the cleavage by Ulp1 did not seem efficient, 1 mM DTT was added into falcons (Addition of DTT can improve cleavage efficiency) during Ulp1-mediated SUMO tag cleavage and was incubated for 2 hours. Rest of the protocol was same as that of trial 1. Protein was eluted in 47 ml after Ni-NTA affinity chromatography (0.4 mg/ml). Even though cleavage efficiency has slightly increased, the amount of protein lost was very high. The final yield of M1-Strep was 0.1 mg/ml.

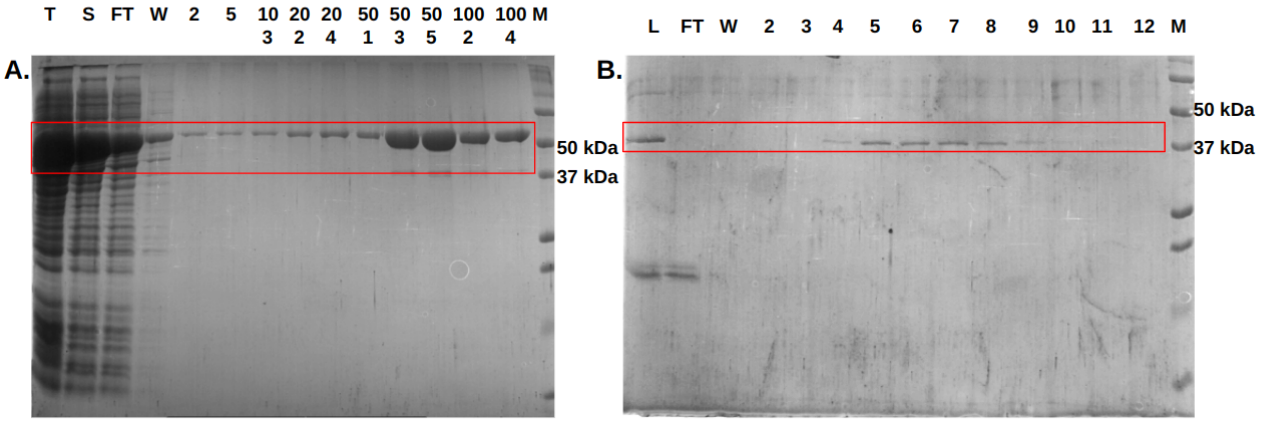

Fig. 3.22: **Trial 2 of large scale SUMO tag cleavage Standardization** A) SDS-PAGE gel image after Ni-NTA purification of $(His)_6$-SUMO-M1-Strep B) SDS-PAGE gel image after Strep affinity purification post SUMO tag cleavage. The expected band size is highlighted within the red box. "T" - Total, "S" - Supernatant, "FT" - Flow through, "W" - Wash, "L" - load (Input for Strep affinity chromatography) & "M" - Ladder

Trial 3:

As the final yield after cleavage was very less, it was decided to process 4 L instead of 2 L. Rest of the protocol was kept the same as that of trial 2. It was clear from the gel that even after processing 4 L pellets, the amount of protein obtained finally was not that different from the previous one because when the amount of $(His)_6$-SUMO-M1-Strep was high, the amount of protein precipitated after cleavage was also high. Another major issue was that the full-length ($(His)_6$-SUMO-M1-Strep) protein was also present along with M1-Strep (protein after cleavage), and this could cause difficulties in quantification for many assays.

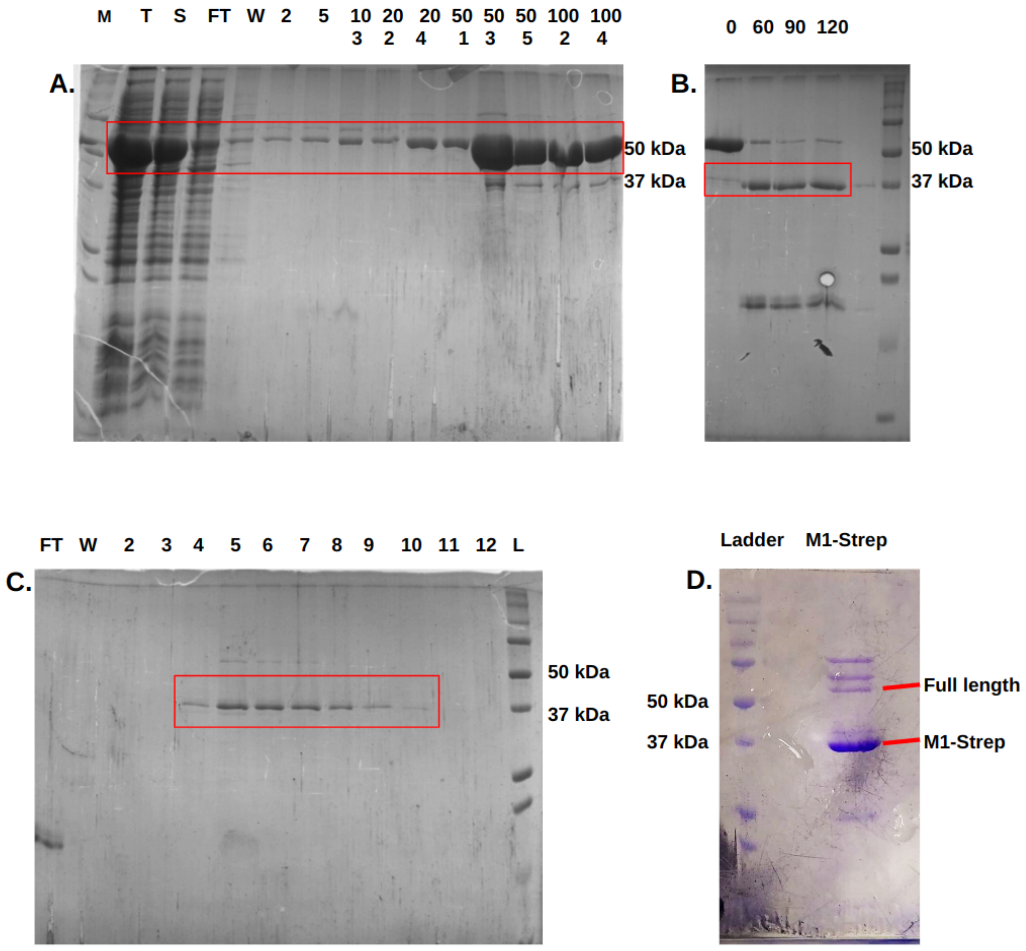

Fig. 3.23: **Trial 3 of large scale SUMO tag cleavage Standardization** A) SDS-PAGE gel image after Ni-NTA purification of $(His)_6$-SUMO-M1-Strep B) Sumo tag cleavage efficiency check at 0, 60, 90 and 120 minutes time point C) SDS-PAGE gel image after Strep affinity purification post SUMO tag cleavage. D) M1-Strep purity check. The expected band size is highlighted within the red box. "T" - Total, "S" - Supernatant, "FT" - Flow through, "W" - Wash & "L" - Ladder.

Trial 4:

A new strategy was tried to separate the full-length protein from the untagged protein (M1-Strep). 1 L pellet of $(His)_6$-SUMO-M1-Strep was resuspended and sonicated, then the supernatant (obtained after the spin) was diluted to 100 ml and then collected in two falcons. To these falcons, Ulp1 protease and DTT (1 mM) were added. The falcons were under shaking conditions at 4 ^{O}C. It started precipitating after 30 minutes, but then

it was spun at 15000 rpm (4 ^{O}C) for one hour, during which further cleavage happened. For purification, the Ni-NTA column (on top) and the Strep-trap column were connected in series and were equilibrated with buffer A (Table 2.14). Once the spin was over, the supernatant was collected and passed on from the NI-NTA column. The idea was that the full-length protein (had Strep-tag as well as His tag) binds to the Ni-NTA column, and the untagged one (which had only the Strep-tag) binds to the Strep-trap column. After loading, the Ni-NTA column was disconnected, and protein was eluted only from the strep-trap column with 2.5 mM D-Desthiobiotin. There was no band for the full-length protein as expected, but the prominent band was around 75 kDa.

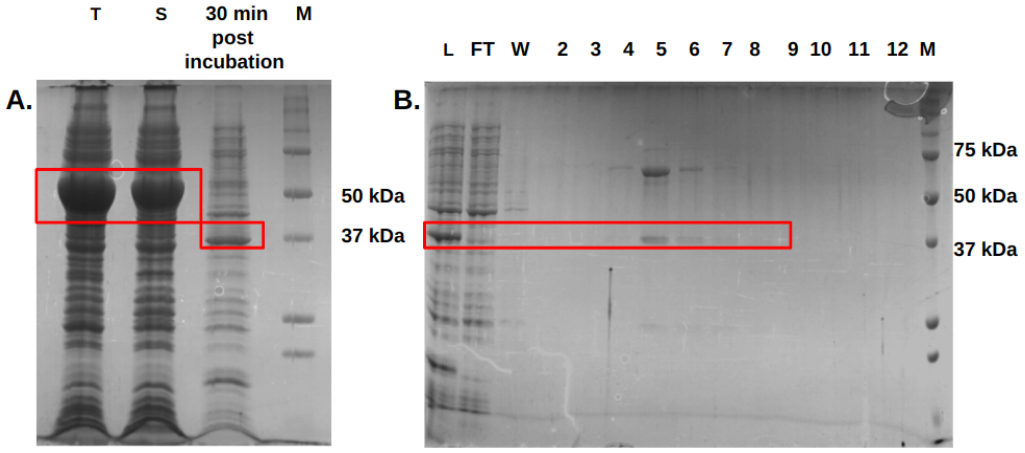

Fig. 3.24: **Trial 4 of large scale SUMO tag cleavage Standardization** A) SDS-PAGE gel image showing SUMO tag cleavage efficiency B) SDS-PAGE gel image of eluted cleaved protein (M1-Strep) from Strep-trap column. The expected band sizes are highlighted within the red box. “T” - Total, “S” - Supernatant, “FT” - Flow through, “W” - Wash, “L” - load (Input provided for the columns connected in parallel) & “M” - Ladder

3.3.8 TEM to visualize ScM1 filaments.

TEM images showed filament formation by ScM1 (Fig. 3.25). The filaments which were visible looked short and straight. It was not very clear whether they formed double protofilaments like other characterized MreBs.

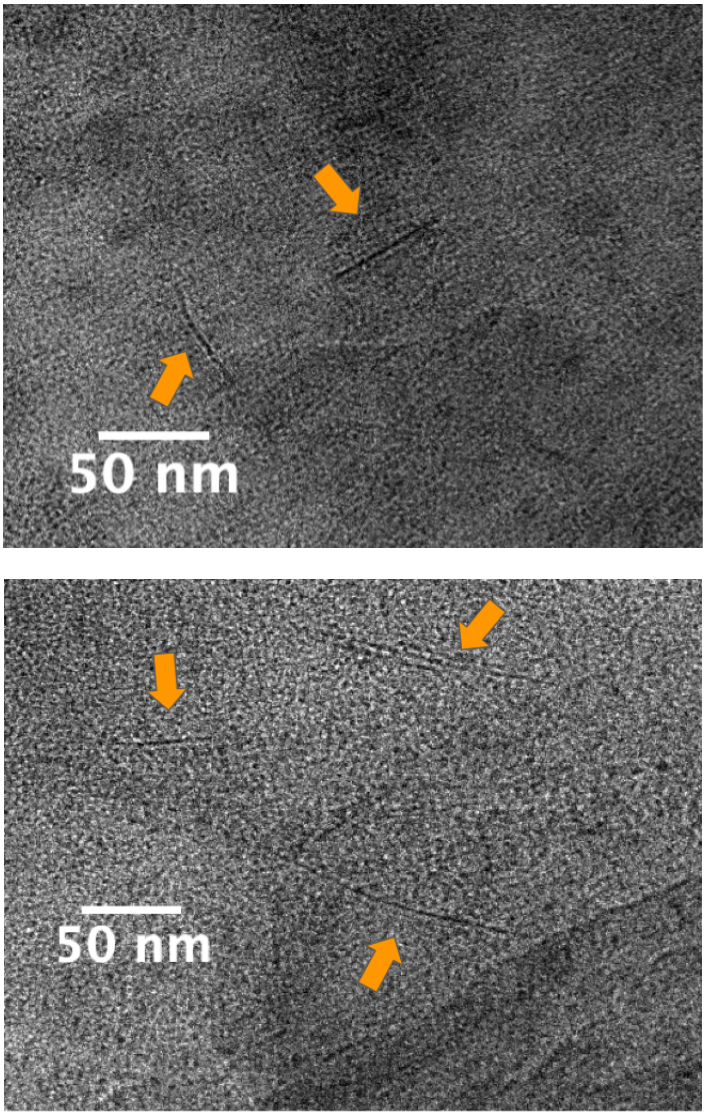

Fig. 3.25: **Visualization of ScM1 filaments using TEM.** Orange arrows point towards the filaments. Both of images were from the same grid (10 µM of $(His)_6$-SUMO-M1-Strep stained by 0.5% uranyl acetate) The TEM images were processed using ImageJ to establish proper scale bars.

3.4 Characterization of $(His)_6$-SUMO-M1-Strep - E137A

Compared to the purity of wild type $(His)_6$-SUMO-M1, the purity of $(His)_6$-SUMO-M1-Strep was better. Also, the ATPase activity of $(His)_6$-SUMO-M1-Strep was higher than that of $(His)_6$-SUMO-M1 and more closer to that of ScM1-$(His)_6$ (0.49 min^{-1}). So it was decided to mutate E137 of $(His)_6$-SUMO-M1-Strep to alanine.

3.4.1 Cloning of $(His)_6$-SUMO-M1-Strep - E137A

pET28a_$(His)_6$-SUMO-M1-Strep was used as template for PCR 1. Primers used for PCR 1 are shown in table 2.1 (sequences in red correspond to gene, blue corresponds to that of pET28a vector, green corresponds to the strep tag and those highlighted in yellow corresponds to the mutation). Around 0.7 Kb amplification was visible on agarose gel after PCR 1 (Fig. 3.26 A). pET28a_$(His)_6$-SUMO-M1-Strep itself was used as template for PCR 2. Details of PCR 1 and PCR 2 are given in tables 2.11, 2.12 and 2.13. After PCR 2, DpnI digestion was done, followed by transformation through electroporation. Test plate had lot of colonies, and control plate was clean. As the template and insert used for PCR 2 had M1 gene, clone check PCR using gene specific primers were of no relevance. Double digestion check was also of no use for the same reason. Three samples were sent for sequencing. One of the clones came positive.

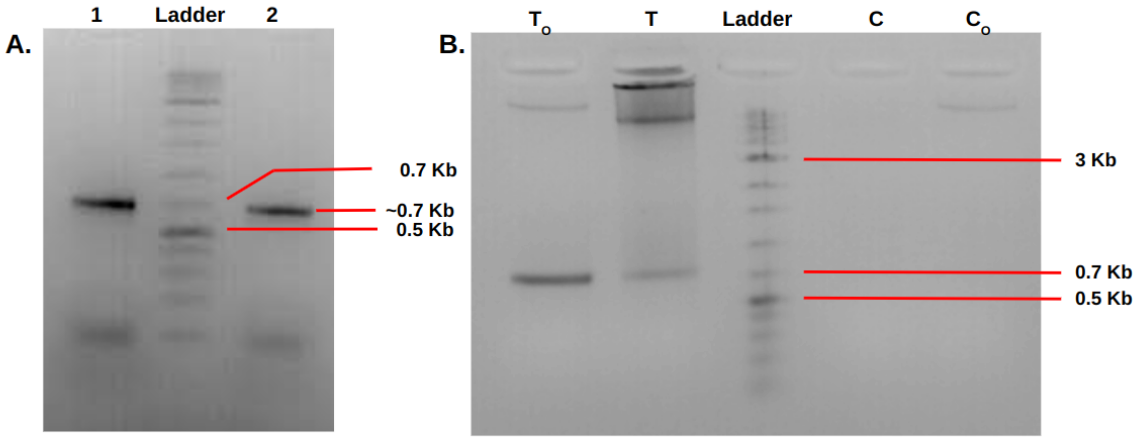

Fig. 3.26: **Cloning of $(His)_6$-SUMO-M1-Strep - E137A.** A) Agarose gel image after PCR 1; 1 & 2 are two 50 µL reactions B) Agarose gel image after PCR 2; (T_0, T, C_0, C - Details are given in section 2.1.2)

3.4.2 Expression check of $(His)_6$ -SUMO-M1-Strep - E137A

pET28a_$(His)_6$-SUMO-M1-Strep - E137A (kanamycin resistant) was transformed into Rosetta (DE3) for expression check. It showed very good expression (Fig. 3.27) and solubility. This was therefore transformed into Rosetta to grow large cultures prior to

protein purification.

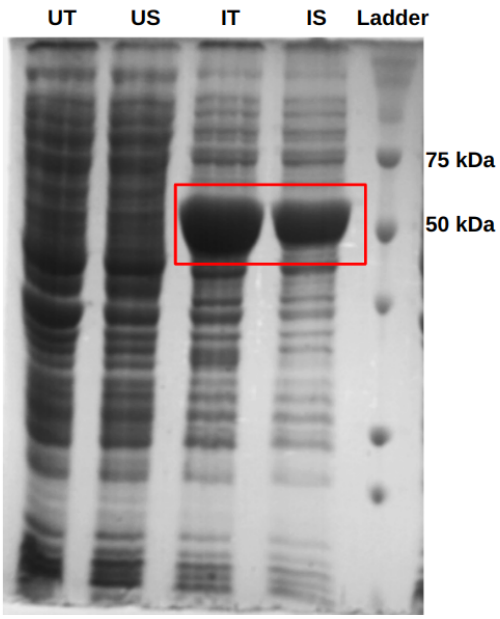

Fig. 3.27: **Expression check of $(His)_6$-SUMO-M1-Strep - E137A.** SDS-PAGE gel image after expression check. The expected band size is highlighted within the red box. “U” - uninduced, “I” - induced, “T” - total, “S” - supernatant

3.4.3 Purification of $(His)_6$ -SUMO-M1-Strep - E137A

1 L culture (Rosetta-DE3) pellet of $(His)_6$-SUMO-M1-Strep - E137A was processed. After Strep affinity chromatography (Fig 3.28), best fractions were pooled together and concentrated. The final yield of protein obtained was 2.6 mg/ml (800 µL).

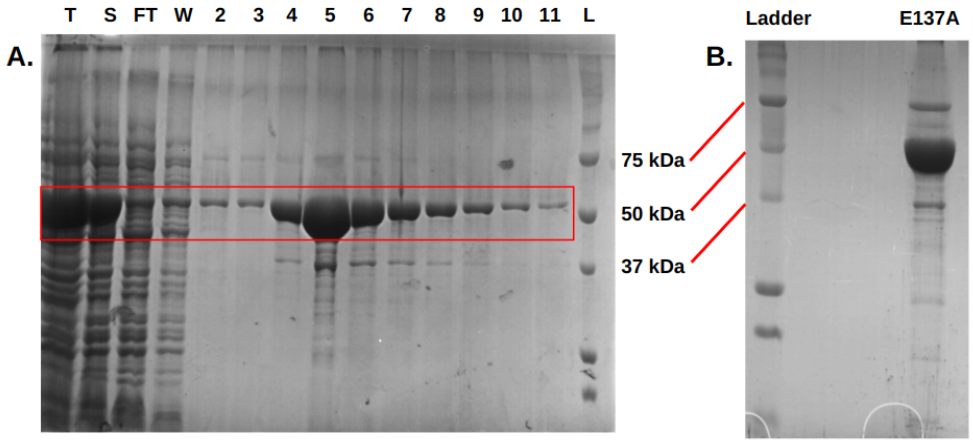

Fig. 3.28: **Purification of $(His)_6$ -SUMO-M1-Strep - E137A.** A) SDS-PAGE gel image after Strep affinity purification. B) SDS-PAGE gel image of purity check. The expected band size is highlighted within the red box. "T" - Total, "S" - Supernatant, "FT" - Flow through, "W" - Wash & "L" - Ladder.

3.4.4 Malachite assay to quantify ATPase activity

Malachite assay was tried for 10 µM of $(His)_6$-SUMO-M1-Strep - E137A. Similar to $(His)_6$-SUMO-M1 - E137, this mutant was also ATPase active. Mean k_{obs} obtained for wild type and mutant are given in table 3.3. Scatter plot is shown in fig. 3.29. 2 way Annova test suggests that there is no significant difference between the activity of wild type and mutant.

Table 3.3: ATPase activity of $(His)_6$-SUMO-M1Strep - E137A

Protein	Concentration (µM)	No. of repeats	k_{obs} (min^{-1})
$(His)_6$-SUMO-M1-Strep	10	4	0.399 ± 0.015
$(His)_6$-SUMO-M1-Strep - E137A	10	2	0.457 ± 0.016

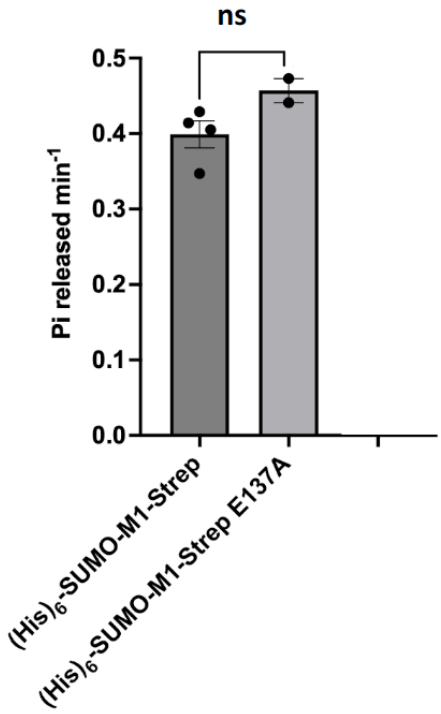

Fig 3.29: **Plot for comparison of ATPase activity of $(His)_6$-SUMO-M1-Strep and $(His)_6$-SUMO-M1-Strep - E137A.** Y-axis shows k_{obs} of $(His)_6$-SUMO-M1-Strep and $(His)_6$-SUMO-M1-Strep - E137A. 2 way Annova test was used to compare the activity between constructs. “ns” refers to “not significant” (p-value = 0.1108).

Chapter - 4
Discussion and Future Prospects

After the cloning of pET28a_$(His)_6$-SUMO-M1, the expression and solubility of ScM1 had increased very much because of the N-terminal fusion of SUMO tag. Compared to the yield usually obtained for the ScM1-$(His)_6$ construct (around 500 µL of 0.7 mg/ml protein from 2L culture), the yield obtained for $(His)_6$-SUMO-M1 was always very high (around 1 ml of 20 mg/ml protein from 1 L culture). With intact SUMO tag, M1 never precipitated at any stage during or after purification. Elution profile was similar for these constructs (spread from void to monomer). Purity wise there wasn't any significant difference between the above mentioned constructs. Among all the constructs made so far, $(His)_6$-SUMO-M1-Strep was the best with respect to purity due to inclusion of Strep affinity purification which is very specific. As the impurity bands were still visible on the SDS-PAGE gel even after consecutive rounds of purification (Ni-NTA followed by Strep affinity chromatography), there is more chance that these impurities were getting bound to the protein and not to the column. Also some of the bands which were visible below the expected size could be some degraded forms of ScM1 itself.

The purification of untagged M1 and M1-Strep from $(His)_6$-SUMO-M1 and $(His)_6$-SUMO-M1-Strep respectively after SUMO tag cleavage was challenging as the protein precipitated after the removal of SUMO tag. Purification of untagged M1 with two rounds of Ni-NTA led to reduction in the yield and also the purified untagged M1 had equal amounts of SUMO tag as well as full length protein. Complete cleavage needed longer incubation or shorter incubation with more amount of of Ulp1 protease but the issue was that either way the amount of protein lost was a lot. Standardization was done in small scale (section 3.1.4) after which the amount of protease (in moles ratio) and incubation time was figured out. But on moving to a larger scale, these did not remain consistent. For the complete removal of SUMO tag, gel filtration was required which again resulted in further loss of protein. Relatively, $(His)_6$-SUMO-M1-Strep was better as a method to remove full length and cleaved SUMO tag from M1-Strep (section

3.3.7). Also, as the protein elutes in lesser volume in the case of Strep affinity chromatography (8-12 ml) compared to Ni-NTA affinity chromatography (~ 50 ml), the centricon based concentrating step was quicker after the introduction of Strep tag. This saved the time and the protein did not have to be out for a long time thereby avoiding chances of degradation. Improving the yield post SUMO tag cleavage is still ongoing. As the protein precipitates in the absence of SUMO tag, ideal buffer conditions have to be identified for solubilizing the untagged protein. Also, purification has to be standardized in terms of improving the purity especially for the SUMO constructs which are fine in terms of expression and solubility.

Thermal shift assay was inconclusive for all the constructs. The sypro orange dye was always getting bound to the protein at the beginning itself and as a result the RFU vs temperature plot never came similar to the standard theoretical curve. There were two possibilities thought to be responsible for this. One is that the protein was not folded properly as a result of which the dye was getting bound at the very start itself. Also, further standardization of this assay might enable this assay to work for this protein.

Malachite Green assay confirmed that the protein was an active ATPase. Even though within a construct, the activity was consistent across different batches of purified protein and different repeats of the assay, it varied across different costructs. The ATPase activity of $(His)_6$-SUMO-M1-Strep was higher than that of $(His)_6$-SUMO-M1. This could be primarily due to the unreliable quantification of protein concentration for the assay because of the presence of impurities. Also, the activity of M1-$(His)_6$ (previously estimated in the lab) was different from these constructs. The mutant version (E137A) of both $(His)_6$-SUMO-M1 and $(His)_6$-SUMO-M1-Strep was ATPase active and the activity was higher than that of the wild type protein. For the M1-$(His)_6$ construct, E137A mutant was ATPase inactive. Since, both $(His)_6$-SUMO-M1 - E137A and $(His)_6$-SUMO-M1-Strep - E137A were showing ATPase activity, it was less likely to be from some impurities. There can be more than one residue involved in ATPase activity and therefore mutating other residues which are catalytically more important can be a solution to this. For example, T167 in CcMreB was shown to be catalytically important (van den Ent et al.,

2014) and when corresponding ScM5 residue (T161) was mutated, it became ATPase inactive (Pande et al., 2022). This Threonine is conserved across all ScMreBs (Except ScMreB3). Mutating this might make the protein ATPase inactive.

Transmission electron micrographs gave a sense that the protein forms short filaments. The presence of filaments were not uniform in grids. This could be due to usage of a lower concentration of protein (10 μM). Another possibility is that some of the protein might have formed aggregates. Improper staining could also be a reason. The protocol for preparation of grids should be standardized in terms of protein concentration, amount of staining and its duration for better visualization of ScM1 filaments. Filament formation can also be checked using TEM after subjecting the protein to different nucleotide conditions.

The ATPase activity shown by the protein, the presence of secondary structure confirmed from CD spectroscopy and the formation of filaments as observed from transmission electron micrographs suggests that the protein is in its folded state. Pelleting assay showed that the protein does not pellet down in the absence or presence of nucleotide while spun at a speed of 100,000 xg. One reason can be because the protein forms shorter filaments which are not denser enough to pellet down at a speed of 100,000 xg. ScM5 was also shown to not pellet on its on irrespective of the nucleotide condition at a speed of 100,000 xg (Pande et al., 2022). Also there are reports suggesting *Spiroplasma eriocheiris* MreB5 and MreB3 pellets after incubation with ATP for 1 hour in the buffer (20 mM Tris-HCl pH 8, 1 M NaCl, 200 mM Arginine-HCl pH 8, 5 mM DTT, 2 mM MgCl2 and 2 mM ATP) and spinning it at 4,36,000 xg for 2 hours at 23 ^{O}C (Takahashi et al., 2022). There is a possibility that ScM1 can also pellet down if spun at a speed of 4,36,000 xg or above with proper incuation after ATP addition. As ScM1 was not pelleting on its own while spun at 100,000 xg irrespective of the presence of nucleotide, co-pelleting (Co-sedmentation) assay can be tried with ScM1 and Fibril to check for possible interaction between these, similar to what was done for ScM5 and Fibril (Harne et al., 2020). Also, liposome pelleting assay can be tried to check whether ScM1 has binding affinity towards lipososmes. High-perfomance

liquid chromatography (HPLC) can be done to find out whether any nucleotide is bound to the protein. Since the protein comes in void while eluting from gel filtration column, it is most likely that the protein forms higher order oligomers. Creation of a polymerization mutant can be thought of a solution for obtaining monomeric ScM1. The residues to be mutated can be figured out via a sequence alignment similar to what was done for designing the ATPase mutant. If monomeric fractions are obtained and if those are of higher concentration, protein can be used to set up crystallization.

Chapter - 5

References

[1] Bean, G. J., & Amann, K. J. (2008). Polymerization properties of the Thermotoga maritima actin MreB: roles of temperature, nucleotides, and ions. Biochemistry, 47(2), 826–835. https://doi.org/10.1021/bi701538e

[2] Berry, C., O'Neil, S., Ben-Dov, E., Jones, A. F., Murphy, L., Quail, M. A., Holden, M. T., Harris, D., Zaritsky, A., & Parkhill, J. (2002). Complete sequence and organization of pBtoxis, the toxin-coding plasmid of Bacillus thuringiensis subsp. israelensis. Applied and environmental microbiology, 68(10), 5082–5095. https://doi.org/10.1128/AEM.68.10.5082-5095.2002

[3] Bork, P., Sander, C., & Valencia, A. (1992). An ATPase domain common to prokaryotic cell cycle proteins, sugar kinases, actin, and hsp70 heat shock proteins. Proceedings of the National Academy of Sciences of the United States of America, 89(16), 7290–7294. https://doi.org/10.1073/pnas.89.16.7290

[4] Cabeen, M. T., & Jacobs-Wagner, C. (2010). The bacterial cytoskeleton. Annual review of genetics, 44, 365–392. https://doi.org/10.1146/annurev-genet-102108-134845

[5] Chou, S. Z., & Pollard, T. D. (2019). Mechanism of actin polymerization revealed by cryo-EM structures of actin filaments with three different bound nucleotides. Proceedings of the National Academy of Sciences of the United States of America, 116(10), 4265–4274. https://doi.org/10.1073/pnas.1807028115

[6]Daniels, M. J., Longland, J. M., & Gilbart, J. (1980). Aspects of motility and chemotaxis in spiroplasmas. Microbiology, 118(2), 429-436.

[7] de Boer, P., Crossley, R., & Rothfield, L. (1992). The essential bacterial cell-division protein FtsZ is a GTPase. Nature, 359(6392), 254–256. https://doi.org/10.1038/359254a0

[8] Dempwolff, F., Reimold, C., Reth, M., & Graumann, P. L. (2011). Bacillus subtilis MreB orthologs self-organize into filamentous structures underneath the cell membrane

in a heterologous cell system. PloS one, 6(11), e27035. https://doi.org/10.1371/journal.pone.0027035

[9] Dominguez, R., & Holmes, K. C. (2011). Actin structure and function. Annual review of biophysics, 40, 169–186. https://doi.org/10.1146/annurev-biophys-042910-155359

[10] Garner, E. C., Campbell, C. S., & Mullins, R. D. (2004). Dynamic instability in a DNA-segregating prokaryotic actin homolog. Science (New York, N.Y.), 306(5698), 1021–1025. https://doi.org/10.1126/science.1101313

[11] Garner, E. C., Campbell, C. S., & Mullins, R. D. (2004). Dynamic instability in a DNA-segregating prokaryotic actin homolog. Science (New York, N.Y.), 306(5698), 1021–1025. https://doi.org/10.1126/science.1101313

[12] Garnier, M., Clerc, M., & Bove, J. M. (1981). Growth and division of spiroplasmas: morphology of Spiroplasma citri during growth in liquid medium. Journal of bacteriology, 147(2), 642–652. https://doi.org/10.1128/jb.147.2.642-652.1981

[13] Gayathri, P., Fujii, T., Møller-Jensen, J., van den Ent, F., Namba, K., & Löwe, J. (2012). A bipolar spindle of antiparallel ParM filaments drives bacterial plasmid segregation. Science (New York, N.Y.), 338(6112), 1334–1337. https://doi.org/10.1126/science.1229091

[14] Gayathri, P., Fujii, T., Namba, K., & Löwe, J. (2013). Structure of the ParM filament at 8.5Å resolution. Journal of structural biology, 184(1), 33–42. https://doi.org/10.1016/j.jsb.2013.02.010

[15] Gilad, R., Porat, A., & Trachtenberg, S. (2003). Motility modes of Spiroplasma melliferum BC3: a helical, wall-less bacterium driven by a linear motor. Molecular microbiology, 47(3), 657–669. https://doi.org/10.1046/j.1365-2958.2003.03200.x

[16] Gitai, Z., Dye, N. A., Reisenauer, A., Wachi, M., & Shapiro, L. (2005). MreB actin-mediated segregation of a specific region of a bacterial chromosome. Cell, 120(3), 329–341. https://doi.org/10.1016/j.cell.2005.01.007

[17] Harne, S., Duret, S., Pande, V., Bapat, M., Béven, L., & Gayathri, P. (2020). MreB5 Is a Determinant of Rod-to-Helical Transition in the Cell-Wall-less Bacterium Spiroplasma. Current biology : CB, 30(23), 4753–4762.e7. https://doi.org/10.1016/j.cub.2020.08.093

[18] Harne, S., Gayathri, P., & Béven, L. (2020). Exploring Spiroplasma Biology: Opportunities and Challenges. Frontiers in microbiology, 11, 589279. https://doi.org/10.3389/fmicb.2020.589279

[19] Izoré, T., Kureisaite-Ciziene, D., McLaughlin, S. H., & Löwe, J. (2016). Crenactin forms actin-like double helical filaments regulated by arcadin-2. eLife, 5, e21600. https://doi.org/10.7554/eLife.21600

[20] Kiyama, H., Kakizawa, S., Sasajima, Y., Tahara, Y. O., & Miyata, M. (2022). Reconstitution of a minimal motility system based on Spiroplasma swimming by two bacterial actins in a synthetic minimal bacterium. Science advances, 8(48), eabo7490. https://doi.org/10.1126/sciadv.abo7490

[21] Komeili, A., Li, Z., Newman, D. K., & Jensen, G. J. (2006). Magnetosomes are cell membrane invaginations organized by the actin-like protein MamK. Science (New York, N.Y.), 311(5758), 242–245. https://doi.org/10.1126/science.1123231

[22] Kruse, T., Bork-Jensen, J., & Gerdes, K. (2005). The morphogenetic MreBCD proteins of Escherichia coli form an essential membrane-bound complex. Molecular microbiology, 55(1), 78–89. https://doi.org/10.1111/j.1365-2958.2004.04367.x

[23] Kürner, J., Frangakis, A. S., & Baumeister, W. (2005). Cryo-electron tomography reveals the cytoskeletal structure of Spiroplasma melliferum. Science (New York, N.Y.), 307(5708), 436–438. https://doi.org/10.1126/science.1104031

[24] Lartigue, C., Lambert, B., Rideau, F., Dahan, Y., Decossas, M., Hillion, M., Douliez, J. P., Hardouin, J., Lambert, O., Blanchard, A., & Béven, L. (2022). Cytoskeletal components can turn wall-less spherical bacteria into kinking helices. Nature communications, 13(1), 6930. https://doi.org/10.1038/s41467-022-34478-0

[25] Löwe, J., He, S., Scheres, S. H., & Savva, C. G. (2016). X-ray and cryo-EM structures of monomeric and filamentous actin-like protein MamK reveal changes associated with polymerization. Proceedings of the National Academy of Sciences of the United States of America, 113(47), 13396–13401. https://doi.org/10.1073/pnas.1612034113

[26]Maeda, Y. T., Nakadai, T., Shin, J., Uryu, K., Noireaux, V., & Libchaber, A. (2012). Assembly of MreB filaments on liposome membranes: a synthetic biology approach. ACS synthetic biology, 1(2), 53–59. https://doi.org/10.1021/sb200003v

[27] Margolin W. (2005). FtsZ and the division of prokaryotic cells and organelles. Nature reviews. Molecular cell biology, 6(11), 862–871. https://doi.org/10.1038/nrm1745

[28] Mayer, J. A., & Amann, K. J. (2009). Assembly properties of the Bacillus subtilis actin, MreB. Cell motility and the cytoskeleton, 66(2), 109–118. https://doi.org/10.1002/cm.20332

[29] Morrison, J. J., Conti, J., & Camberg, J. L. (2022). Assembly and architecture of Escherichia coli divisome proteins FtsA and FtsZ. The Journal of biological chemistry, 298(3), 101663. https://doi.org/10.1016/j.jbc.2022.101663

[30] Muñoz-Espín, D., Daniel, R., Kawai, Y., Carballido-López, R., Castilla-Llorente, V., Errington, J., Meijer, W. J., & Salas, M. (2009). The actin-like MreB cytoskeleton organizes viral DNA replication in bacteria. Proceedings of the National Academy of Sciences of the United States of America, 106(32), 13347–13352. https://doi.org/10.1073/pnas.0906465106

[31]Orlova, A., Garner, E. C., Galkin, V. E., Heuser, J., Mullins, R. D., & Egelman, E. H. (2007). The structure of bacterial ParM filaments. Nature structural & molecular biology, 14(10), 921–926. https://doi.org/10.1038/nsmb1300

[32] Ozyamak, E., Kollman, J., Agard, D. A., & Komeili, A. (2013). The bacterial actin MamK: in vitro assembly behavior and filament architecture. The Journal of biological chemistry, 288(6), 4265–4277. https://doi.org/10.1074/jbc.M112.417030

[33] Pande, V., Mitra, N., Bagde, S. R., Srinivasan, R., & Gayathri, P. (2022). Filament organization of the bacterial actin MreB is dependent on the nucleotide state. The Journal of cell biology, 221(5), e202106092. https://doi.org/10.1083/jcb.202106092

[34] Pollard T. D. (1986). Rate constants for the reactions of ATP- and ADP-actin with the ends of actin filaments. The Journal of cell biology, 103(6 Pt 2), 2747–2754. https://doi.org/10.1083/jcb.103.6.2747

[35] Pollard, T. D., & Cooper, J. A. (2009). Actin, a central player in cell shape and movement. Science (New York, N.Y.), 326(5957), 1208–1212. https://doi.org/10.1126/science.1175862

[36] Ramond, E., Maclachlan, C., Clerc-Rosset, S., Knott, G. W., & Lemaitre, B. (2016). Cell Division by Longitudinal Scission in the Insect Endosymbiont Spiroplasma poulsonii. mBio, 7(4), e00881-16. https://doi.org/10.1128/mBio.00881-16

[37] Razin, S., Hasin, M., Ne'eman, Z., & Rottem, S. (1973). Isolation, chemical composition, and ultrastructural features of the cell membrane of the mycoplasma-like organism Spiroplasma citri. Journal of bacteriology, 116(3), 1421–1435. https://doi.org/10.1128/jb.116.3.1421-1435.1973

[38] Ridley, A., & Heald, R. (2011). Cell structure and dynamics. Current opinion in cell biology, 23(1), 1–3. https://doi.org/10.1016/j.ceb.2010.12.003

[39] Salje, J., van den Ent, F., de Boer, P., & Löwe, J. (2011). Direct membrane binding by bacterial actin MreB. Molecular cell, 43(3), 478–487. https://doi.org/10.1016/j.molcel.2011.07.008

[40] Sasajima, Y., & Miyata, M. (2021). Prospects for the Mechanism of Spiroplasma Swimming. Frontiers in microbiology, 12, 706426. https://doi.org/10.3389/fmicb.2021.706426

[41] Shi, H., Bratton, B. P., Gitai, Z., & Huang, K. C. (2018). How to Build a Bacterial Cell: MreB as the Foreman of E. coli Construction. Cell, 172(6), 1294–1305. https://doi.org/10.1016/j.cell.2018.02.050

[42] Sontag, C. A., Sage, H., & Erickson, H. P. (2009). BtubA-BtubB heterodimer is an essential intermediate in protofilament assembly. PloS one, 4(9), e7253. https://doi.org/10.1371/journal.pone.0007253

[43] Soufo, H. J., & Graumann, P. L. (2010). Bacillus subtilis MreB paralogues have different filament architectures and lead to shape remodelling of a heterologous cell system. Molecular microbiology, 78(5), 1145–1158. https://doi.org/10.1111/j.1365-2958.2010.07395.x

[44] Steinberg, T. H., Haugland, R. P., & Singer, V. L. (1996). Applications of SYPRO orange and SYPRO red protein gel stains. Analytical biochemistry, 239(2), 238–245. https://doi.org/10.1006/abio.1996.0320

[45] Swulius, M. T., & Jensen, G. J. (2012). The helical MreB cytoskeleton in Escherichia coli MC1000/pLE7 is an artifact of the N-Terminal yellow fluorescent protein tag. Journal of bacteriology, 194(23), 6382–6386. https://doi.org/10.1128/JB.00505-12

[46] Szwedziak, P., & Löwe, J. (2013). Do the divisome and elongasome share a common evolutionary past?. Current opinion in microbiology, 16(6), 745–751. https://doi.org/10.1016/j.mib.2013.09.003

[47] Szwedziak, P., Wang, Q., Freund, S. M., & Löwe, J. (2012). FtsA forms actin-like protofilaments. The EMBO journal, 31(10), 2249–2260. https://doi.org/10.1038/emboj.2012.76

[48] Takahashi, D., Fujiwara, I., Sasajima, Y., Narita, A., Imada, K., & Miyata, M. (2022). ATP-dependent polymerization dynamics of bacterial actin proteins involved in Spiroplasma swimming. Open biology, 12(10), 220083. https://doi.org/10.1098/rsob.220083

[49] van den Ent, F., & Löwe, J. (2000). Crystal structure of the cell division protein FtsA from Thermotoga maritima. The EMBO journal, 19(20), 5300–5307. https://doi.org/10.1093/emboj/19.20.5300

[50] van den Ent, F., Izoré, T., Bharat, T. A., Johnson, C. M., & Löwe, J. (2014). Bacterial actin MreB forms antiparallel double filaments. eLife, 3, e02634. https://doi.org/10.7554/eLife.02634

[51] van den Ent, F., Johnson, C. M., Persons, L., de Boer, P., & Löwe, J. (2010). Bacterial actin MreB assembles in complex with cell shape protein RodZ. The EMBO journal, 29(6), 1081–1090. https://doi.org/10.1038/emboj.2010.9

[52] Wagstaff, J., & Löwe, J. (2018). Prokaryotic cytoskeletons: protein filaments organizing small cells. Nature reviews. Microbiology, 16(4), 187–201. https://doi.org/10.1038/nrmicro.2017.153

[53] Young, C. L., Britton, Z. T., & Robinson, A. S. (2012). Recombinant protein expression and purification: a comprehensive review of affinity tags and microbial applications. Biotechnology journal, 7(5), 620–634. https://doi.org/10.1002/biot.201100155

[54] Zepeda Gurrola, R. C., Fu, Y., Rodríguez Luna, I. C., Benítez Cardoza, C. G., López López, M. J., López Vidal, Y., Gutíerrez, G. R. A., Rodríguez Pérez, M. A., & Guo, X. (2017). Novel protein interactions with an actin homolog (MreB) of Helicobacter pylori determined by bacterial two-hybrid system. Microbiological research, 201, 39–45. https://doi.org/10.1016/j.micres.2017.04.008